

Supporting Information

Structure-Property Relationships from Atomistic Multiscale Simulations of the Relevant Processes in Organic Solar Cells

I. Thermodynamic Aspects

Charlotte Brückner[†], Frank Würthner[‡], Klaus Meerholz[#], Bernd Engels,[†]

[†] Institut für Theoretische Chemie, Universität Würzburg, Emil-Fischer-Straße 42, 97074 Würzburg, Germany

[‡] Institut für Organische Chemie, Universität Würzburg, Am Hubland, 97074 Würzburg, Germany

[#] Department Chemie, Universität zu Köln, Luxemburgerstr. 116, 50939 Köln, Germany

E-Mail: bernd.engels@uni-wuerzburg.de,

phone number: (+49) 931 - 31 – 85394,

fax number: (+49) 931 - 31 - 85331

Content

1. Selection of the dimers: distance thresholds
2. Effective epsilon values used to include the environment
3. Calculation of the interfacial electric fields
4. Horizontal dimensions of the simulated interfacial cells
5. Calculated energetic profiles for all crystallographic orientations and all molecules

Figure S2: anthracene:fullerene (a-b)

Figure S3: anthracene:fullerene (a-c)

Figure S4: DIP:fullerene (b-c)

Figure S5: HB194:fullerene (a-c)

Figure S6: HB194:fullerene (b-c)

Figure S7: MD353:fullerene (a-c)

Figure S8: MD353:fullerene (b-c)

Figure S9: diketopyrrolopyrrole:fullerene (a-c)

Figure S10: diketopyrrolopyrrole:fullerene (b-c)

Figure S11: rubrene:fullerene (a-b)

Figure S12: rubrene:fullerene (a-c)

Figure S13: rubrene:fullerene (b-c)

Figure S14: squaraine:fullerene (a-c)

Figure S15: squaraine:fullerene (b-c)

Figure S16: TAA:fullerene (a-b)

Figure S17: TAA:fullerene (a-c)

Figure S18: TAA:fullerene (b-c)

Figure S19: TBA:fullerene (a-b)

Figure S20: TBA:fullerene (b-c)

Figure S21: TAM:fullerene (a-c)

Figure S22: TAM:fullerene (b-c)

6. Influence of the interfacial electric field on the interfacial excitation energies of representative systems

7. Evaluation of the calculated interfacial charge-transfer energies

8. Exemplary calculation of charge transport states at the DIP:fullerene interface

9. Outline of adopted methods used to calculate the states

10. Mass densities of generated interfacial model systems and comparison to bulk-phase densities

Distances used for cutting out the dimers

QM-based dimer calculations were performed for each pair whose distance between the centers of mass is smaller than the corresponding distance thresholds (Table S1). In some cases, the distances depend on the crystallographic orientation to take all important dimers into account.

Table S1: Threshold distances for the dimer selection.

p-type molecule	plane	max. distance "homodimers" [Å]	max. distance "heterodimers" [Å]	max. distance "fullerenes" [Å]
anthracene	a-b	5.5	11.0	10.0
	a-c	5.5	11.0	10.0
	b-c	5.5	11.0	10.0
diketopyrrolopyrrole	a-b	10.0	16.0	10.0
	a-c	13.0	16.0	10.0
	b-c	13.0	14.0	10.0
DIP	a-b	7.0	12.0	10.0
	a-c	7.0	12.0	10.0
	b-c	7.0	12.0	10.0
HB194	a-b	8.0	12.0	10.0
	a-c	8.0	12.0	10.0
	b-c	8.0	12.0	10.0
MD353	a-b	8.0	12.0	10.0
	a-c	8.0	12.0	10.0
	b-c	8.0	12.0	10.0
rubrene	a-b	11.0	12.0	10.0
	a-c	11.0	12.0	10.0
	b-c	11.0	14.0	10.0
squaraine	a-b	10.0	13.0	10.0
	a-c	10.0	13.0	10.0
	b-c	10.0	13.0	10.0
triarylamine (TBA)	a-b	10.0	12.0	10.0
	a-c	10.0	12.0	10.0
	b-c	10.0	13.0	10.0
aldehyde-sub. triarylamine (TAA)	a-b	8.0	11.0	10.0
	a-c	8.0	11.0	10.0
	b-c	8.0	11.0	10.0
methoxy-sub. triarylamine (TAM)	a-b	9.0	12.0	10.0
	a-c	9.0	12.0	10.0
	b-c	9.0	12.0	10.0

Values for the effective epsilon used to mimic the polarizable thin-film environment

Table S2: Effective epsilon values used for the simulation of environmental effects. For COSMO,^{1,2} we used the numerical values while the parameters of the respective solvents were used for PCM.^{3,4}

Molecule	ϵ (p-type)	ϵ (interface)	ϵ (interface, Coulomb)	ϵ (fullerene)
anthracene	2.2706 (benzene)	3.22 (trichloroethane)	2	4.547 (iodobenzene)
diketopyrrolopyrrole	13.580 (cyclopentanone)	9.063 (dichloromethane)	5	4.547 (iodobenzene)
DIP	2.2706 (benzene)	3.22 (trichloroethane)	2	4.547 (iodobenzene)
HB194	20.493 (acetone)	12.440 (m-cresol)	7	4.547 (iodobenzene)
MD353	20.493 (acetone)	12.440 (m-cresol)	7	4.547 (iodobenzene)
rubrene	2.2706 (benzene)	3.22 (trichloroethane)	2	4.547 (iodobenzene)
squaraine	13.580 (cyclopentanone)	9.063 (dichloromethane)	5	4.547 (iodobenzene)
triarylamine (TBA)	5.960 (n-methylaniline)	5.395 (bromobenzene)	3	4.547 (iodobenzene)
aldehyde-sub. triarylamine (TAA)	5.960 (n-methylaniline)	5.395 (bromobenzene)	3	4.547 (iodobenzene)
methoxy-sub. triarylamine (TAM)	5.960 (n-methylaniline)	5.395 (bromobenzene)	3	4.547 (iodobenzene)

The fullerene value is taken from experimental measurements.^{5,6} All numerical values or solvents are selected so that the structural motifs of the solvent were as similar as possible to the soluted p-type semiconducting molecule. For example, the effective epsilon of n-methylaniline is used to simulate the environment of triphenylamine-based compounds. A polar solvent like acetone is used to simulate the merocyanine bulk phase.⁷ The average of the epsilon value for the fullerene bulk phase and the epsilon value of the p-type semiconducting molecule is used for the interfacial region. When calculating Coulombic attraction forces directly at the interface, this epsilon is divided by two to mimic the influence of the less dense packing at the interface on the consequently reduced shielding of the Coulomb interactions.

Estimation of interfacial dipole moments and calculation of electric field strengths via classical electrochemical considerations

It is known from spectroscopic measurements and computations that interfaces give rise to interfacial dipoles and local electric fields that contribute (or impede) to the generation of a charge-transfer state across the interface.⁸ In order to model these local electric fields, a constant electric field is applied for excited-state calculations at the interface.

The field strength of this electric field is calculated as follows: In a first step, the dipole moments of different heterodimers composed of a fullerene and a p-type semiconducting molecule are calculated using ESP charges from the RI⁹-BLYP^{10,11,12}-D3¹³/cc-pVDZ¹⁴ density (MARIJ approximation¹⁵). The charges on each monomer were summed to a total charge Q . As the dimer is neutral, the charges on the respective monomers are equal, but of opposite sign. In the next step the various Q of monomers of different pairs were averaged.

The dipole moments at the interface form an electric dipole layer. Hence, the interface can be modeled as a parallel plate capacitor. According to classical electrochemistry (see ¹⁶), the electric field \vec{E} resulting from the surface distribution of charges Q at each side of the interface is given as

$$\vec{E} = \frac{Q}{\epsilon_0 \epsilon_r \vec{A}} \quad (\text{Eq. 1})$$

In our problem, Q is the given average charge of the monomers, while \vec{A} is the surface area of one dipole moment, i.e., it depends on the density of the packing at the interface. This density is dominated by the bulky shape of the fullerene. Hence we assume one dipole moment per unit cell of the fullerene. The length of the three crystallographic axes of the fullerene ccp crystal structure is $l = 14.04078\text{\AA}$.¹⁷ Assuming a slight density decrease at the interface, which is to be expected, the area of the parallel-plate capacitors can be estimated as

$$|\vec{A}| = 15\text{\AA} \cdot 15\text{\AA} = 225 \cdot 10^{-20} m^2 \quad (\text{Eq. 3})$$

Inserting the charge, the surface area and the vacuum permittivity into the Eq. 1 for the electric field yields Eq. 4, allowing for a calculation of the electric field strength $|\vec{E}|$ generated by the dipole layer.

$$|\vec{E}| = \frac{Q \cdot 1.602 \cdot 10^{-19} C}{8.85 \cdot 10^{-12} \frac{As}{Vm} \cdot 225 \cdot 10^{-20} m^2} \quad (\text{Eq. 4})$$

As already pointed out by Castet et al.,¹⁸ the individual dipole moments of the pairs vary considerably. This can be also seen in Table S3 which shows two extreme values for each p-type semiconductor. We took the average because it is impossible to include all electric dipole fields individually. Moreover, the inclusion of an anisotropic epsilon to model dielectric variations at the interface was computationally not feasible.

Table S3: Charge distributions of two different representative heterodimers for each p-type semiconducting molecule according with the average used in the calculation of the electric field strength. All values are given in a.u.

Molecule	Q(dimer 1)	Q(dimer 2)	Q(average)
anthracene	0.2749	0.0418	0.16
diketopyrrolopyrrole	0.2919	0.0192	0.16
DIP	0.2268	0.2190	0.22
HB194	0.0230	0.3092	0.17
MD353	0.0647	0.1411	0.10
rubrene	0.2013	0.1869	0.19
squaraine	0.0311	0.0898	0.06
triarylamine (TBA)	0.0242	0.1858	0.10
aldehyde-sub. triarylamine (TAA)	0.1663	0.0513	0.10
methoxy-sub. triarylamine (TAM)	0.0995	0.0905	0.10

Please note that the final electric field strength is used in units of $10^{-4} a.u. = 0.0051422 \frac{V}{\text{\AA}}$. Table S4 displays electric field strengths used in the subsequent QM calculations.

Table S4: Electric field strengths in a.u. used in the QM calculations.

Molecule	electric field [0.0001 a.u.]
anthracene	25
diketopyrrolopyrrole	25
DIP	34
HB194	27
MD353	16
rubrene	30
squaraine	9
triarylamine (TBA)	16
aldehyde-sub. triarylamine (TAA)	16
methoxy-sub. triarylamine (TAM)	16

Adjustment of OPLS-AA^{19,20} parameters for the force-field calculations

For all molecules, standard OPLS-AA parameters were used. To ensure the overall charge neutrality of the molecules, excess charges had to be redistributed over neighboring atoms. To check whether this approximative approach significantly influences resulting interface structures, we computed the influence of the charge parameters on the final structures using DIP, the squaraine, and MD353.

In a first step, we assigned our modified OPLS charges as well as Mulliken, Hirshfeld,²¹ CM5,²² and ESP charges²³ obtained in B3LYP²⁴-D3/cc-pVDZ calculations to the molecules. Separate molecular dynamic (MD) simulations were conducted for each set of charges. In this work, the MD simulations were only performed to obtain amorphous structures. Hence we are only interested in the amount of disorder resulting from the different sets of charge parameters. As the disorder parameter we define the orientations of the planar π -systems because the positions of the π -conjugated systems with respect to each other are most decisive for energies and couplings of the dimers (see for example ²⁵). We calculated the orientations of the π -systems as the tilting angles of the molecular planes with respect to the a-b-, a-c- or b-c-plane (Figure S1). In the case of the three-dimensional triarylaminines we use the plane of the central nitrogen atom with the adjacent carbon atoms. In a crystal all orientations are exactly equal, hence no disorder exists. This is reflected in the standard deviations of the tilting angles, which are zero for all crystals. In an amorphous system obtained in an MD simulation the standard deviations of the tilting angles increase. Thus the standard deviation is a measure of the disorder. We calculated the disorder, i.e., the standard deviations of tilting angles, for various MD runs.

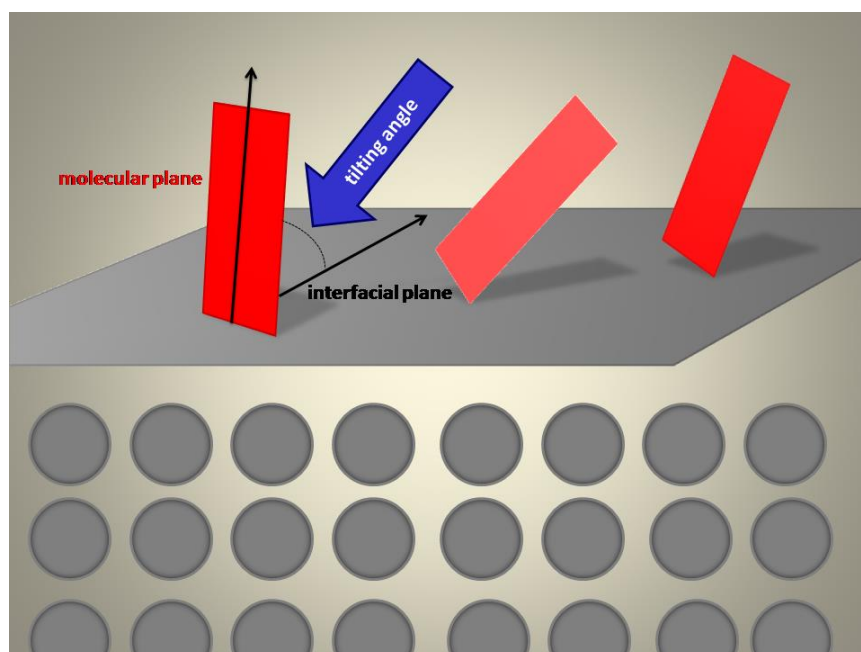


Figure S1: Visualization of the tilting angle as a measure for the molecular orientation and the reorientation taking place during the MD simulations.

The disorder is determined by the employed charge model but depends also on the MD trajectory itself because MD simulations (with long simulation times) are non-deterministic due to the summation of the numerical errors.²⁶ In order to differentiate between both aspects, we performed three different MD simulations using the same OPLS parameters. The values for DIP, the squaraine, and MD353 are given in Table S5 to Table S7, respectively.

Table S5: Obtained distributions of tilting angles of the molecular planes with respect to a reference plane for different DIP interfaces as a function of the employed charge parameters. The first line indicates the method used to obtain atomic charges. “OPLS-1”, “OPLS-2”, and “OPLS-3” indicate three MD simulations using the same modified OPLS-AA parameters.

charges	Mulliken	Hirshfeld	CM5	Esp	OPLS-1	OPLS-2	OPLS-3
a-b [°]	18	20	18	16	15	17	11
a-c [°]	38	52	29	36	33	37	40
b-c [°]	51	48	45	47	43	53	50
Mean [°]	35	40	31	33	31	36	34

Table S6: Obtained distributions of tilting angles of the molecular planes with respect to a reference plane for different squaraine interfaces as a function of the employed charge parameters. The first line indicates the method used to obtain atomic charges. “OPLS-1”, “OPLS-2”, and “OPLS-3” indicate three MD simulations using the same modified OPLS-AA parameters.

charges	Mulliken	Hirshfeld	CM5	Esp	OPLS-1	OPLS-2	OPLS-3
a-b [°]	43	50	47	39	60	50	57
a-c [°]	40	41	33	28	31	30	41
b-c [°]	51	48	42	59	57	35	58
Mean [°]	45	46	40	42	49	38	52

Table S7: Obtained distributions of tilting angles of the molecular planes with respect to a reference plane for different MD353 interfaces as a function of the employed charge parameters. The first line indicates the method used to obtain atomic charges. “OPLS-1”, “OPLS-2”, and “OPLS-3” indicate three MD simulations using the same modified OPLS-AA parameters.

charges	Mulliken	Hirshfeld	CM5	Esp	OPLS-1	OPLS-2	OPLS-3
a-b [°]	16	19	17	18	38	38	38
a-c [°]	27	28	29	29	28	38	22
b-c [°]	36	28	27	34	46	38	44
Mean [°]	26	25	24	27	37	38	35

Please note that for all molecules, the variations in the disorder between the MD simulations using the same parameter set (OPLS-1, OPLS-2, OPLS-3) vary nearly as much or even more than between MD simulations with different charge parameter sets. Taking DIP (Table S5) as an example, the disorder of the tilting angles with respect to the a-b-plane varies between 16° and 20° if different charge models are employed. Using the same parameter set but performing three independent MD simulations (OPLS-1, OPLS-2, OPLS-3), the disorder of the tilting angles varies between 17° and 11°, i.e., the influence of the charge model on the disorder is similar to the variations found due to the non-deterministic behavior of the MD simulation. This shows that our force field approach is sufficiently accurate for the purpose of generating disordered interface structures.

As p-type semiconducting molecules like squaraines and triarylaminines are not necessarily properly described by OPLS-AA, we replaced the computed OPLS-AA geometries by *ab initio* geometries in the subsequent dimer calculations.

Horizontal dimensions of the simulated interfacial cells

As outlined in the paper, the dimensions of the interface are determined as the least common multiple of the crystallographic axes of the crystal structures of the p-type semiconducting molecules and fullerene. Horizontal dimensions as a multiple of the fullerene crystal structure¹⁷ are given in Table S8.

Table S8: Horizontal dimensions of the interfacial cells used in the simulations determined as multiples of the crystallographic axes of fullerene (14.04 Å)¹⁷. The vertical dimension always amounts to approximately four layers of each component (i.e., of the fullerene phase and the p-type semiconducting layer, respectively).

Molecule	plane	dimension 1 [Å]	dimension 2 [Å]
anthracene	a-b	42	42
	a-c	42	42
	b-c	42	42
diketopyrrolopyrrole	a-b	28	42
	a-c	28	28
	b-c	42	28
DIP	a-b	28	42
	a-c	28	84
	b-c	42	84
HB194	a-b	42	42
	a-c	42	70
	b-c	42	70
MD353	a-b	70	42
	a-c	70	28
	b-c	42	28
rubrene	a-b	28	28
	a-c	28	28
	b-c	28	28
squaraine	a-b	28	98
	a-c	28	28
	b-c	98	28
triarylamine (TBA)	a-b	42	42
	a-c	42	42
	b-c	42	42
aldehyde-sub. triarylamine (TAA)	a-b	28	56
	a-c	28	42
	b-c	56	42
methoxy-sub. triarylamine (TAM)	a-b	42	42
	a-c	42	98
	b-c	42	98

Calculated energetic profiles for all crystallographic orientations and all molecules

For comparison and completeness, all energetic profiles not shown in the manuscript are shown in the following figures, Figure S2 to Figure S24. The symbols are assigned to the different states in Table 1.

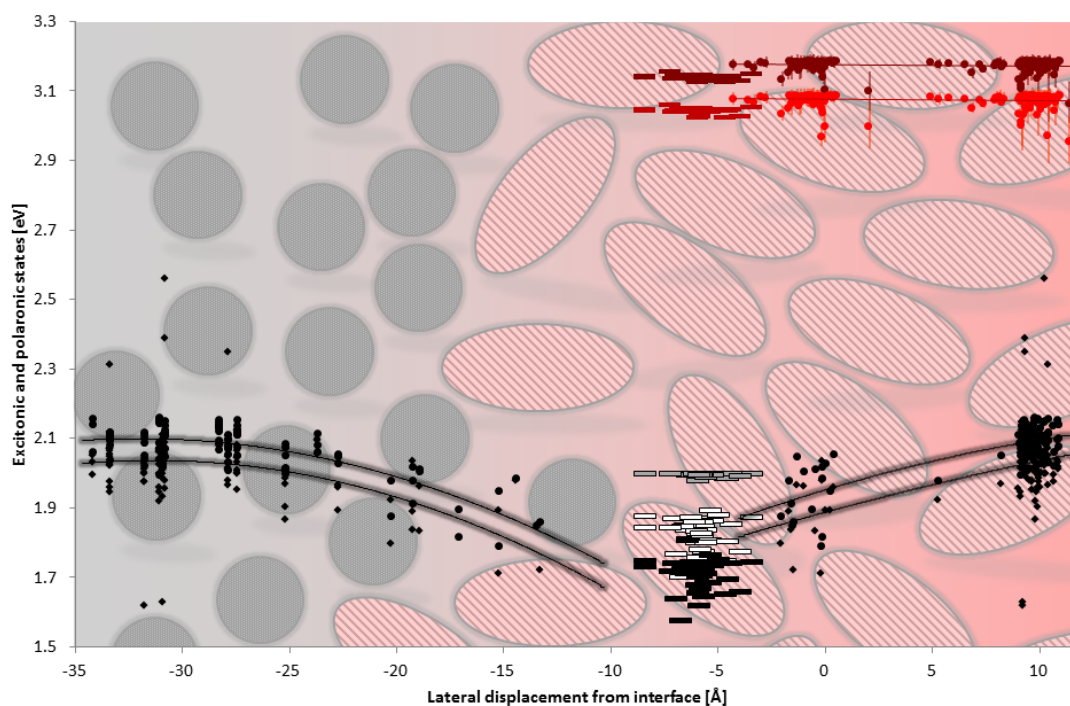


Figure S2: Energetic profile along the anthracene:fullerene interface (a-b-crystallographic plane).

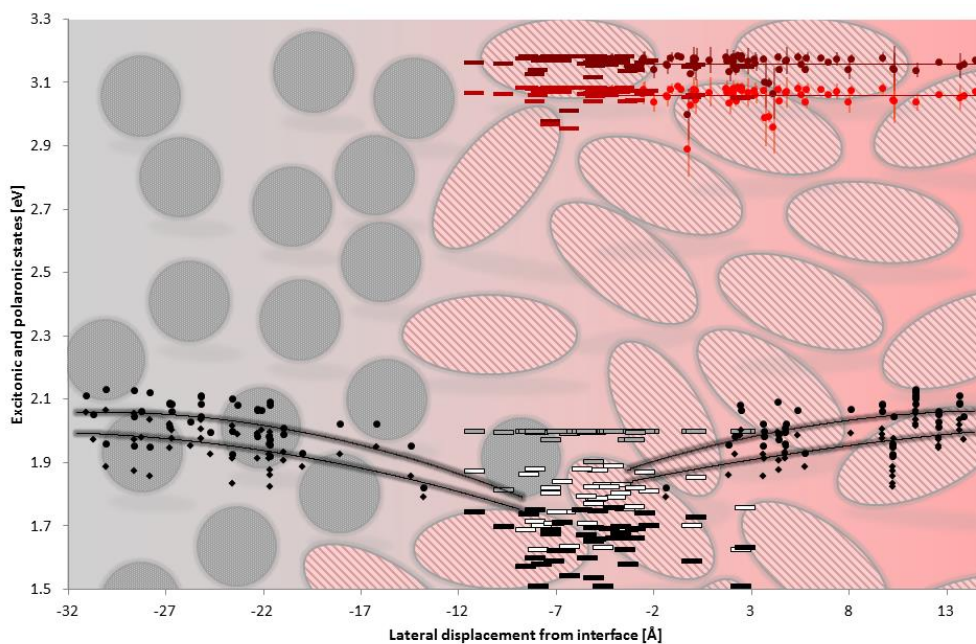


Figure S3: Energetic profile along the anthracene:fullerene interface (a-c-crystallographic plane).

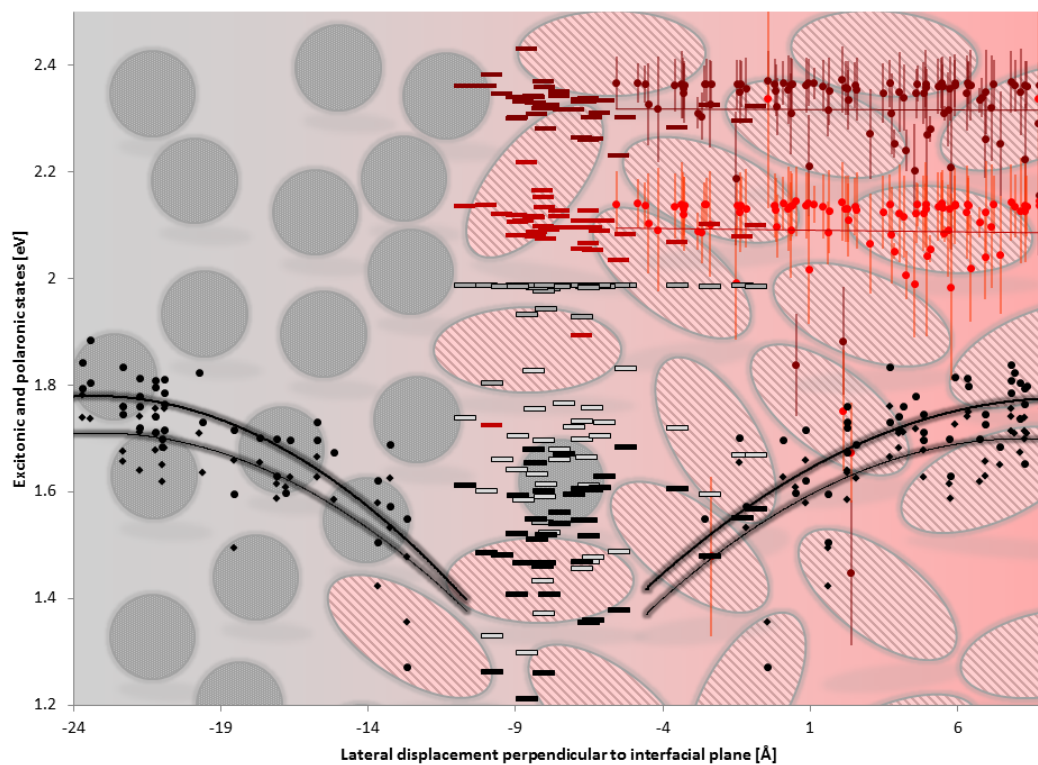


Figure S4: Energetic profile along the DIP:fullerene interface (b-c-crystallographic plane).

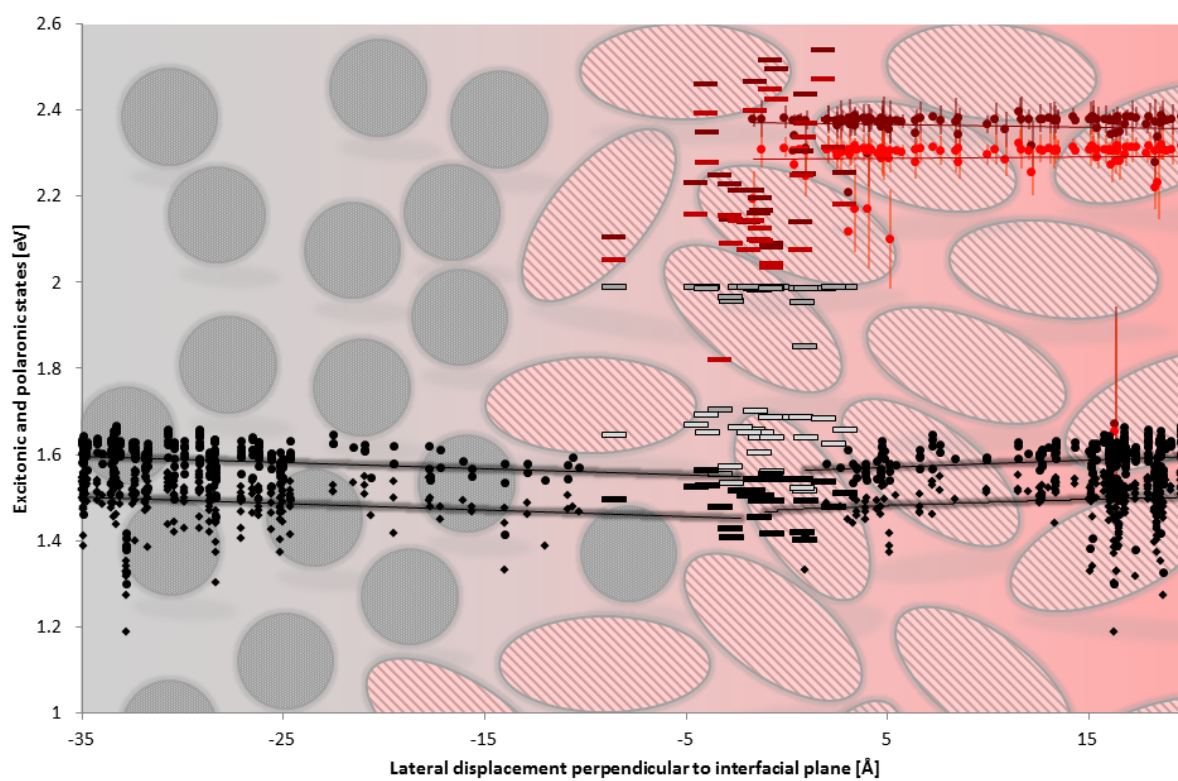


Figure S5: Energetic profile along the HB194:fullerene interface (a-c-crystallographic plane).

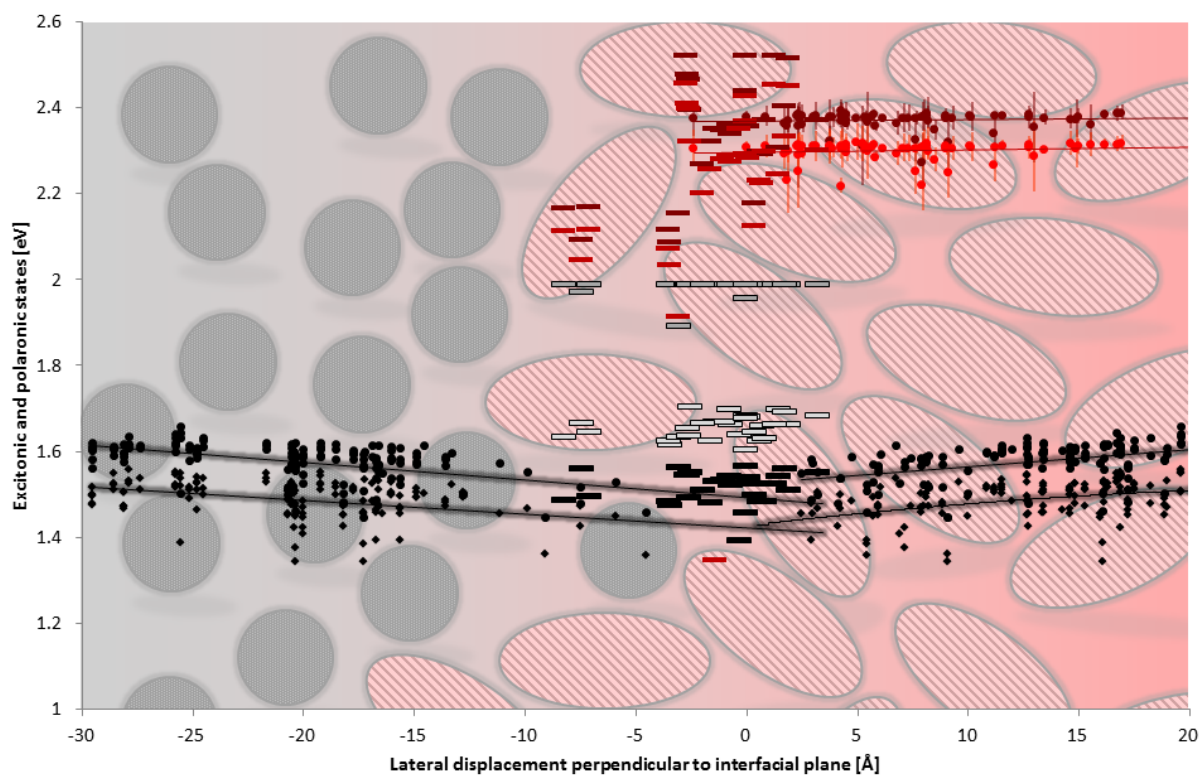


Figure S6: Energetic profile along the HB194:fullerene interface (b-c-crystallographic plane).

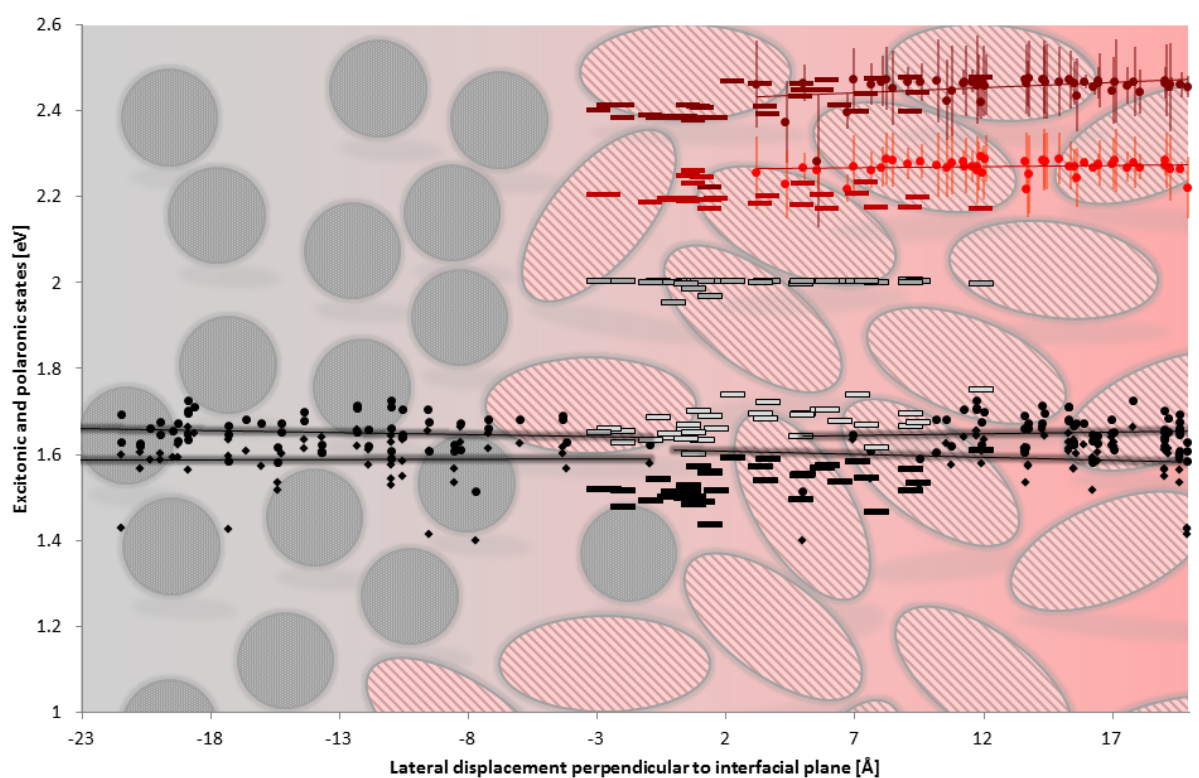


Figure S7: Energetic profile along the MD353:fullerene interface (a-c-crystallographic plane).

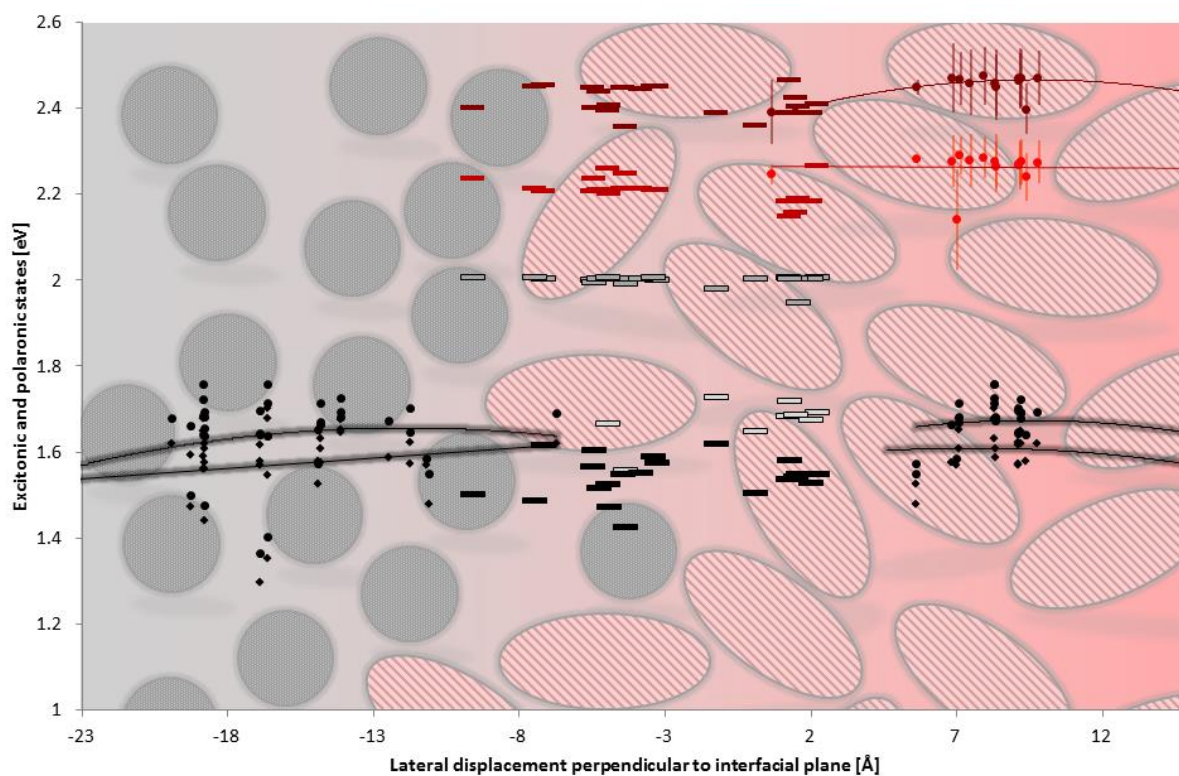


Figure S8: Energetic profile along the MD353:fullerene interface (b-c-crystallographic plane).

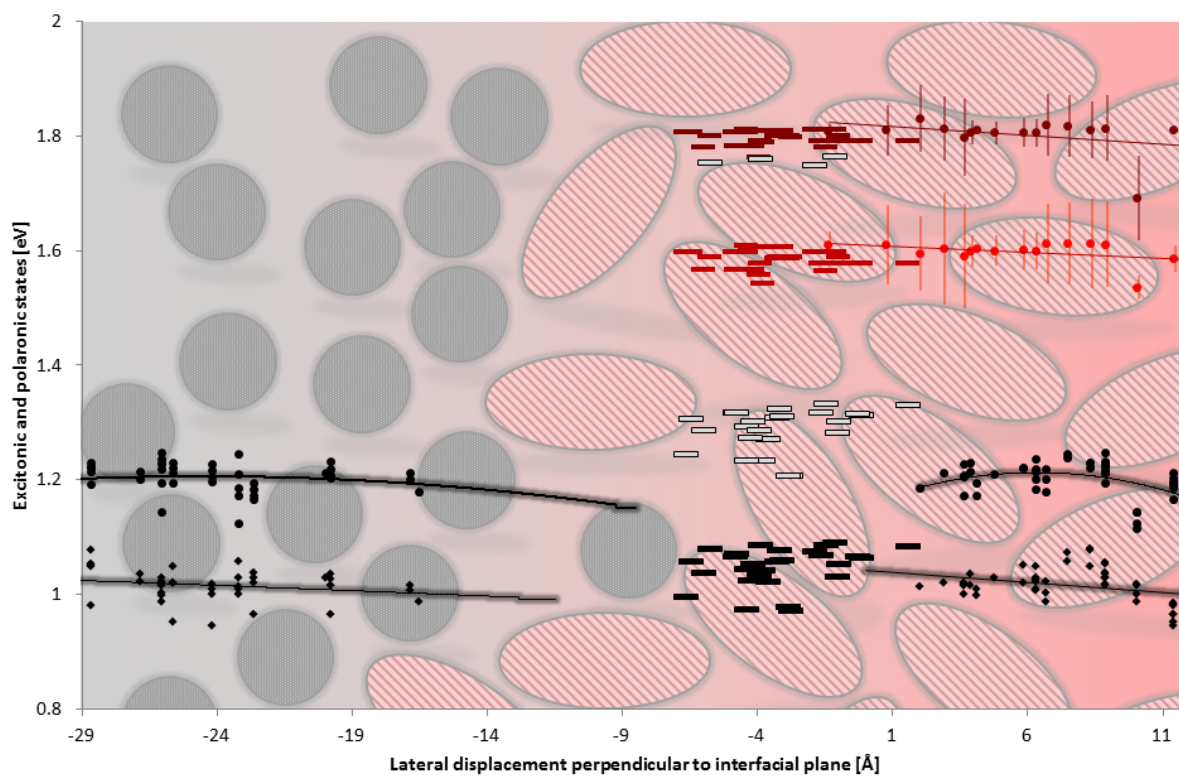


Figure S9: Energetic profile along the diketopyrrolopyrrole:fullerene interface (a-c-crystallographic plane).

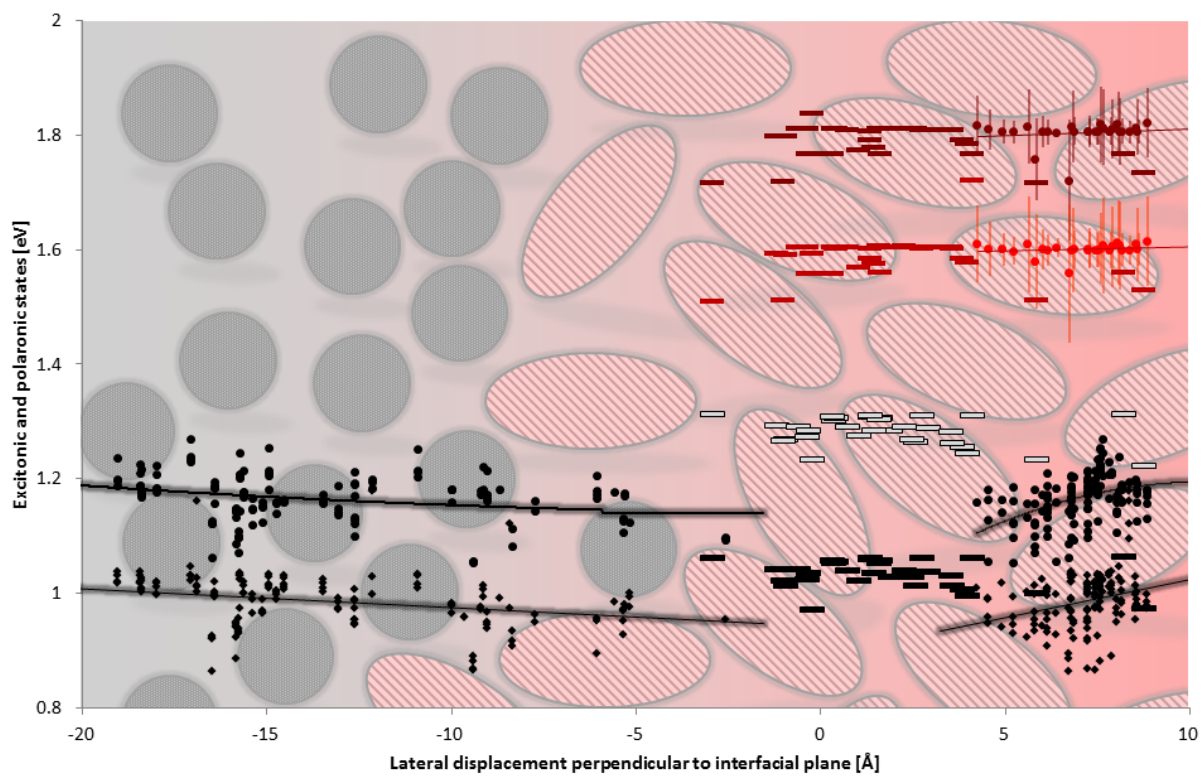


Figure S10: Energetic profile along the diketopyrrolopyrrole:fullerene interface (b-c-crystallographic plane).

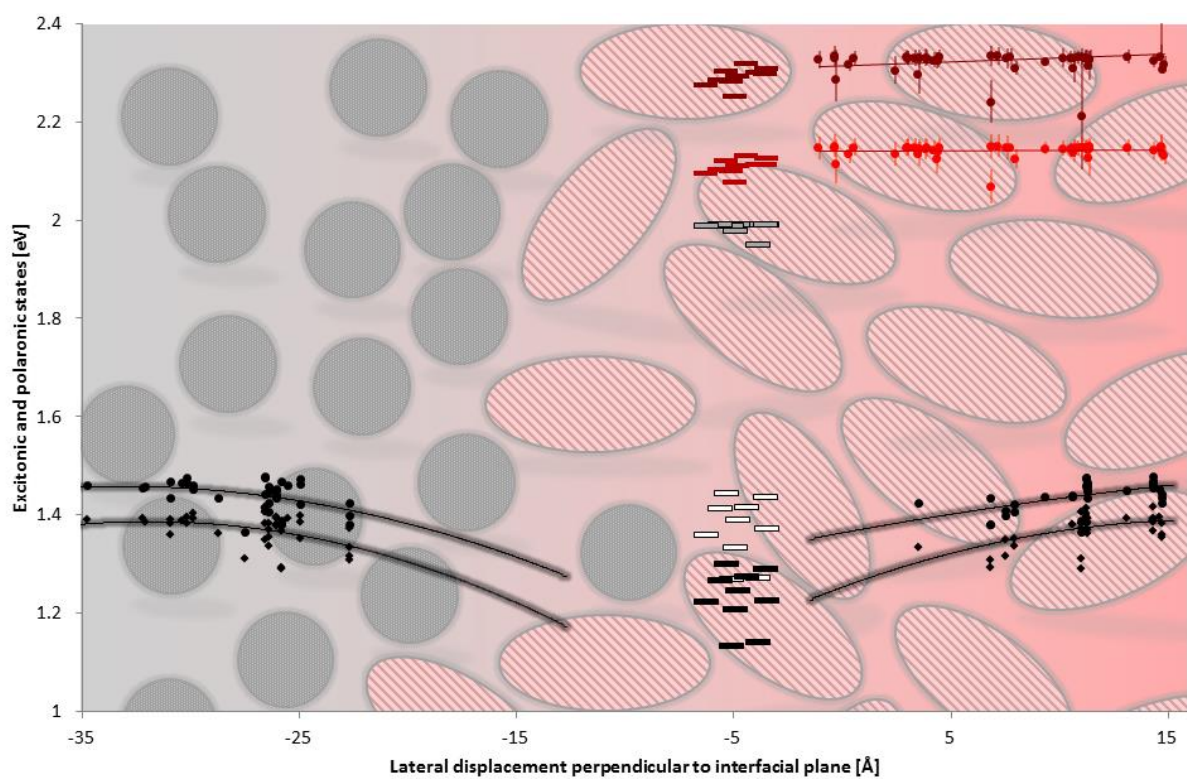


Figure S11: Energetic profile along the rubrene:fullerene interface (a-b-crystallographic plane).

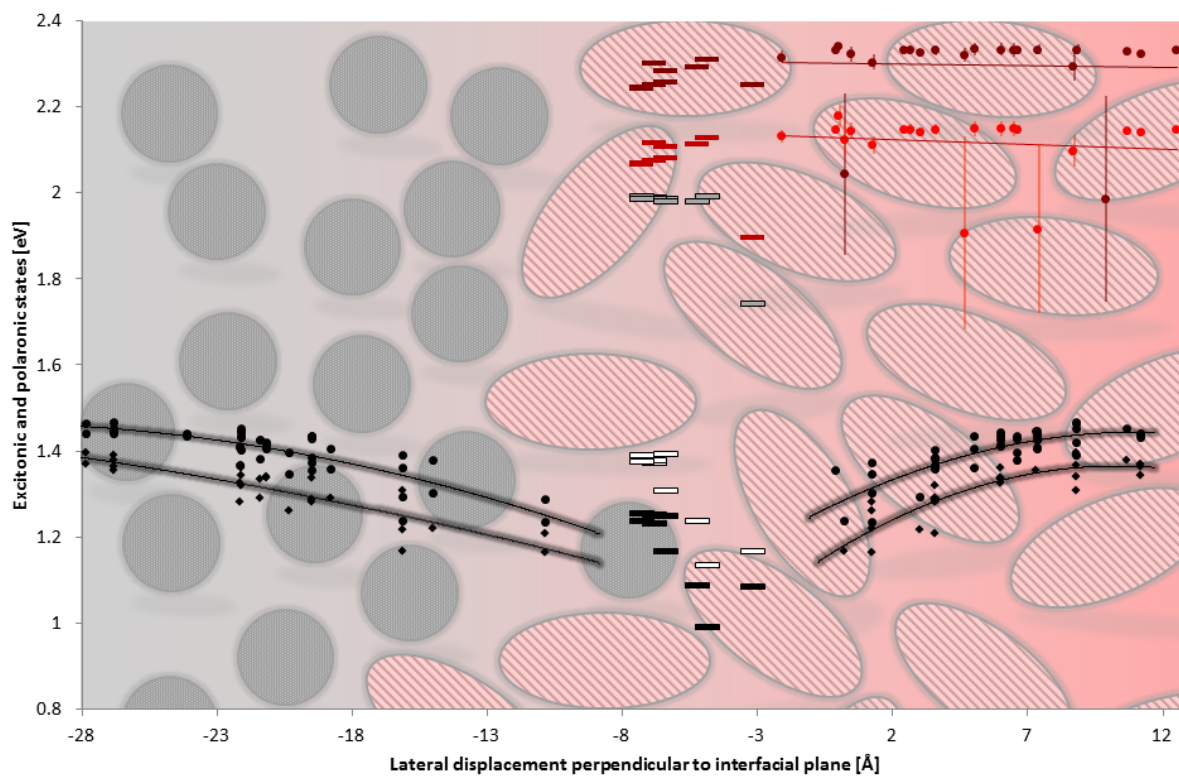


Figure S12: Energetic profile along the rubrene:fullerene interface (a-c-crystallographic plane).

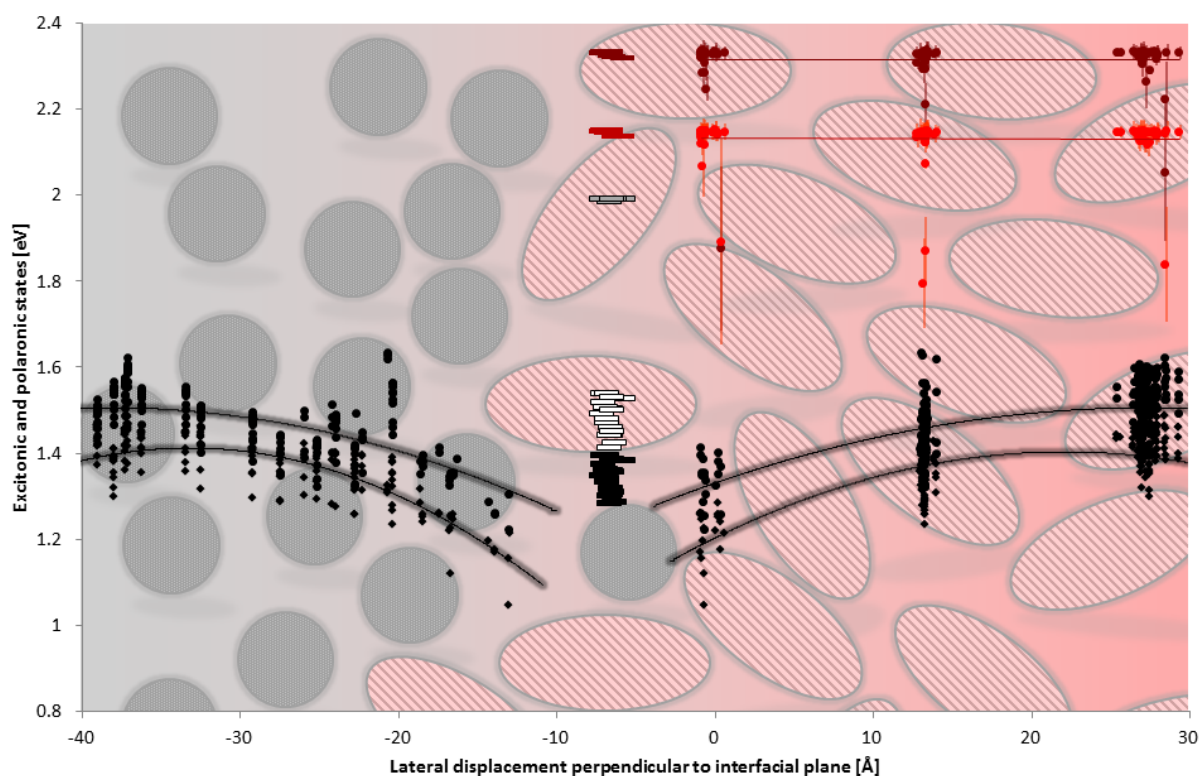


Figure S13: Energetic profile along the rubrene:fullerene interface (b-c-crystallographic plane).

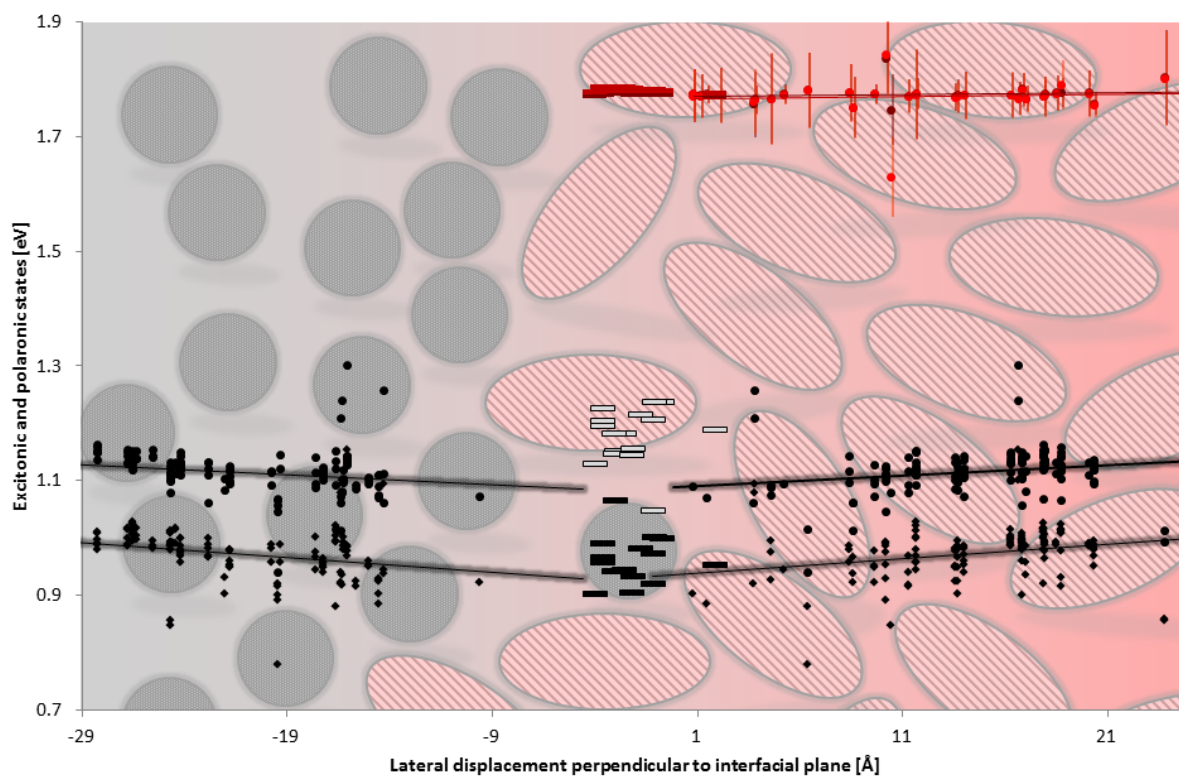


Figure S14: Energetic profile along the squaraine:fullerene interface (a-c-crystallographic plane).

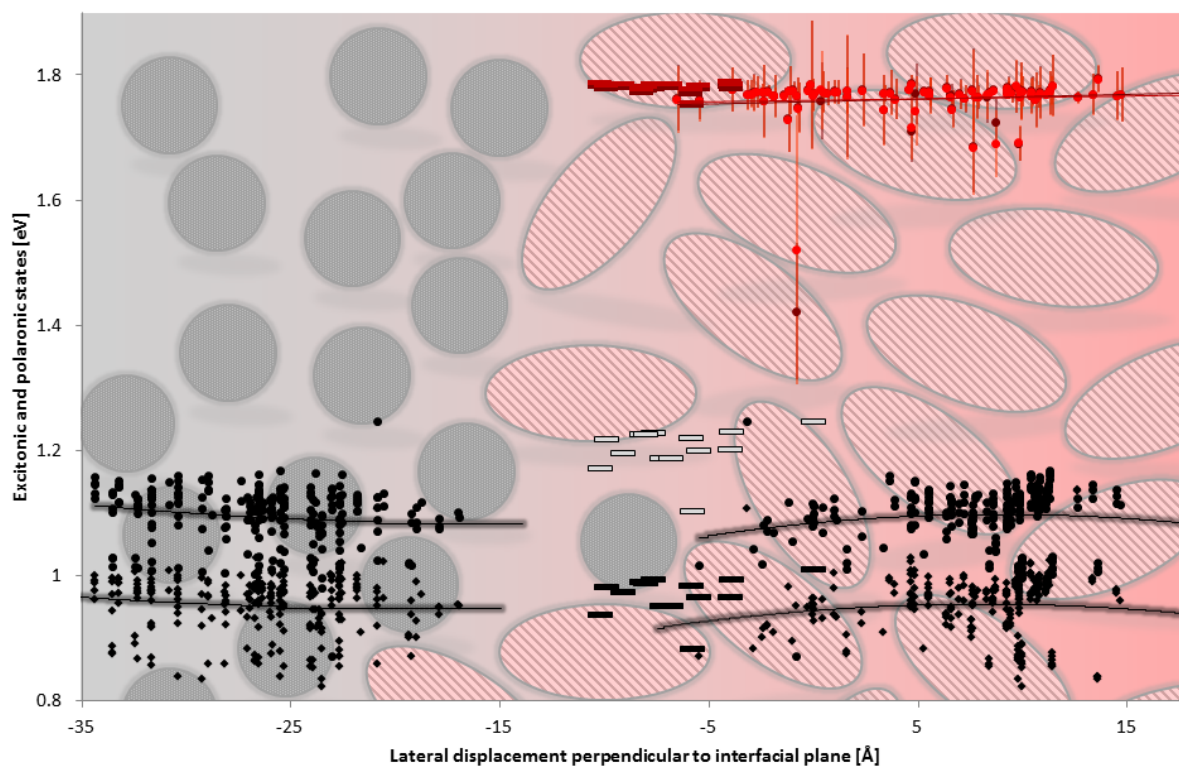


Figure S15: Energetic profile along the squaraine:fullerene interface (b-c-crystallographic plane).

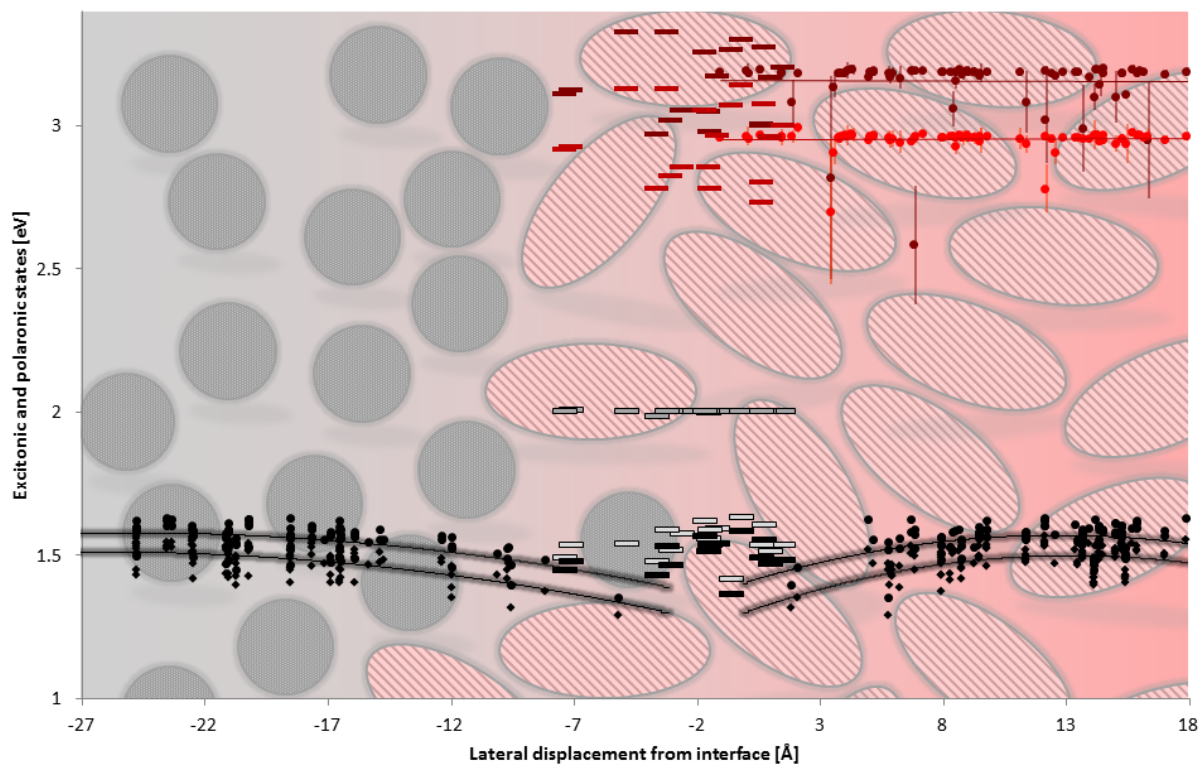


Figure S16: Energetic profile along the TAA:fullerene interface (a-b-crystallographic plane).

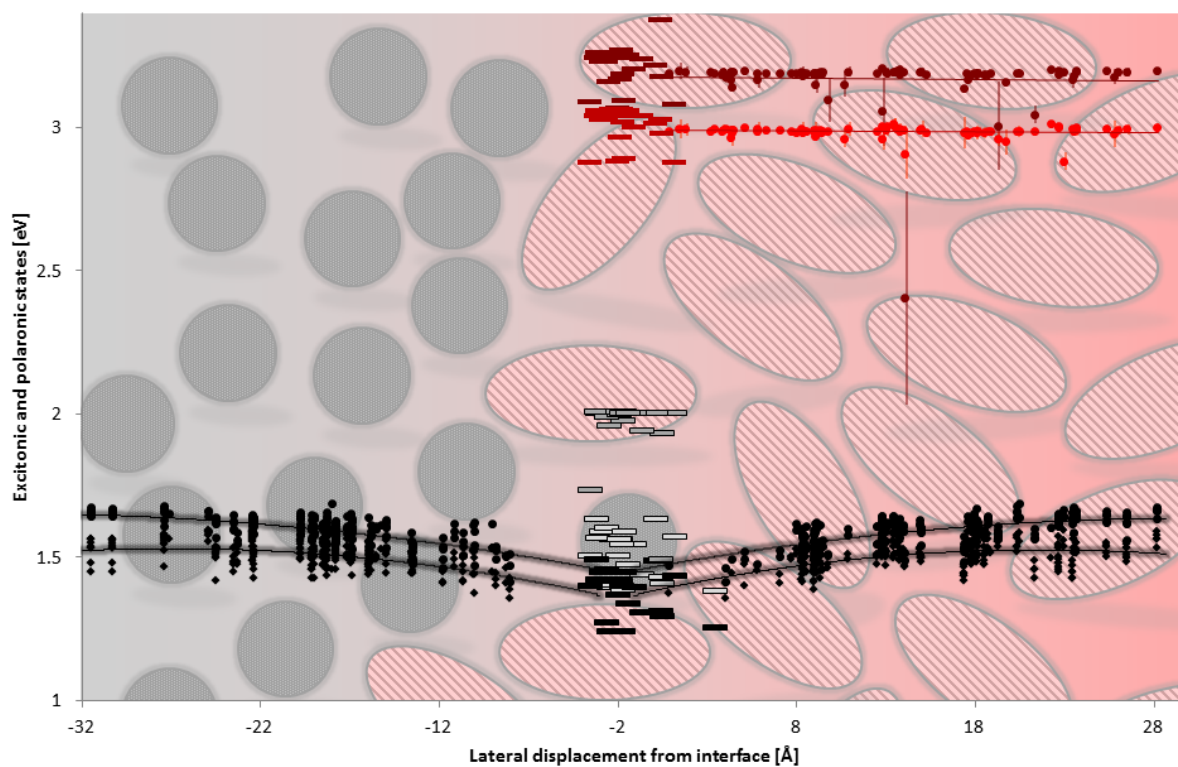


Figure S17: Energetic profile along the TAA:fullerene interface (a-c-crystallographic plane).

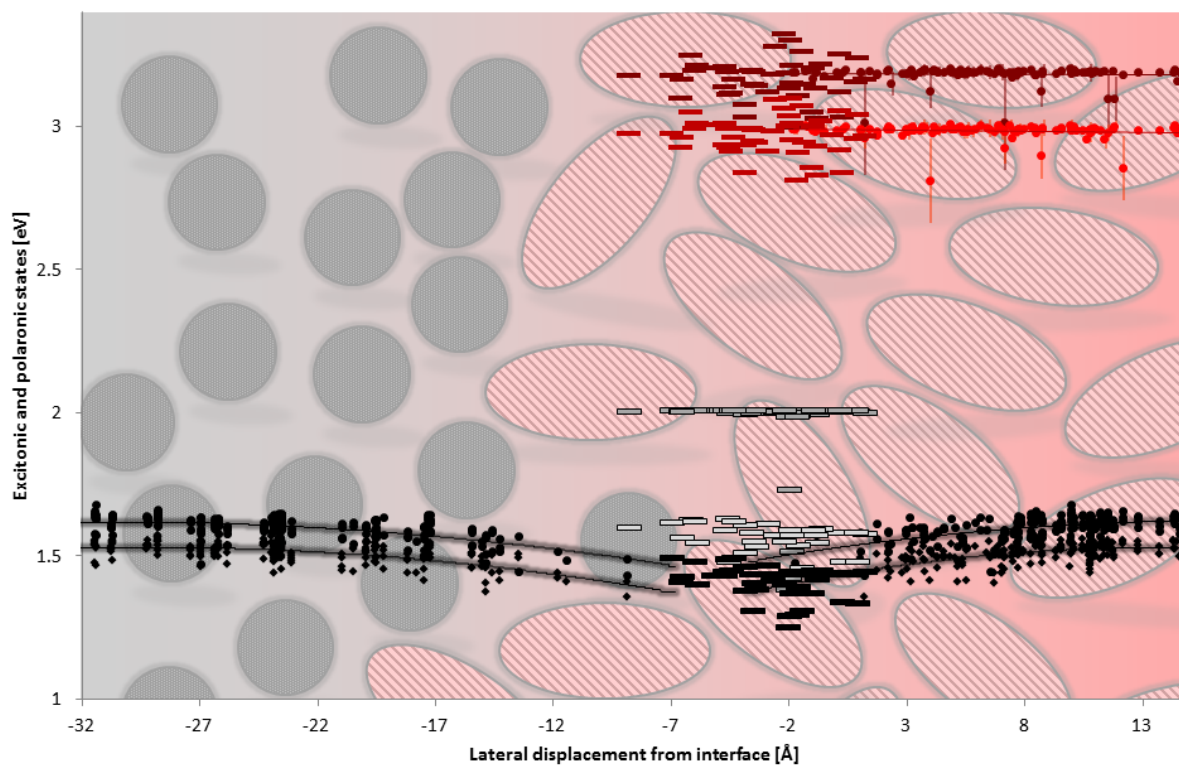


Figure S18: Energetic profile along the TAA:fullerene interface (b-c-crystallographic plane).

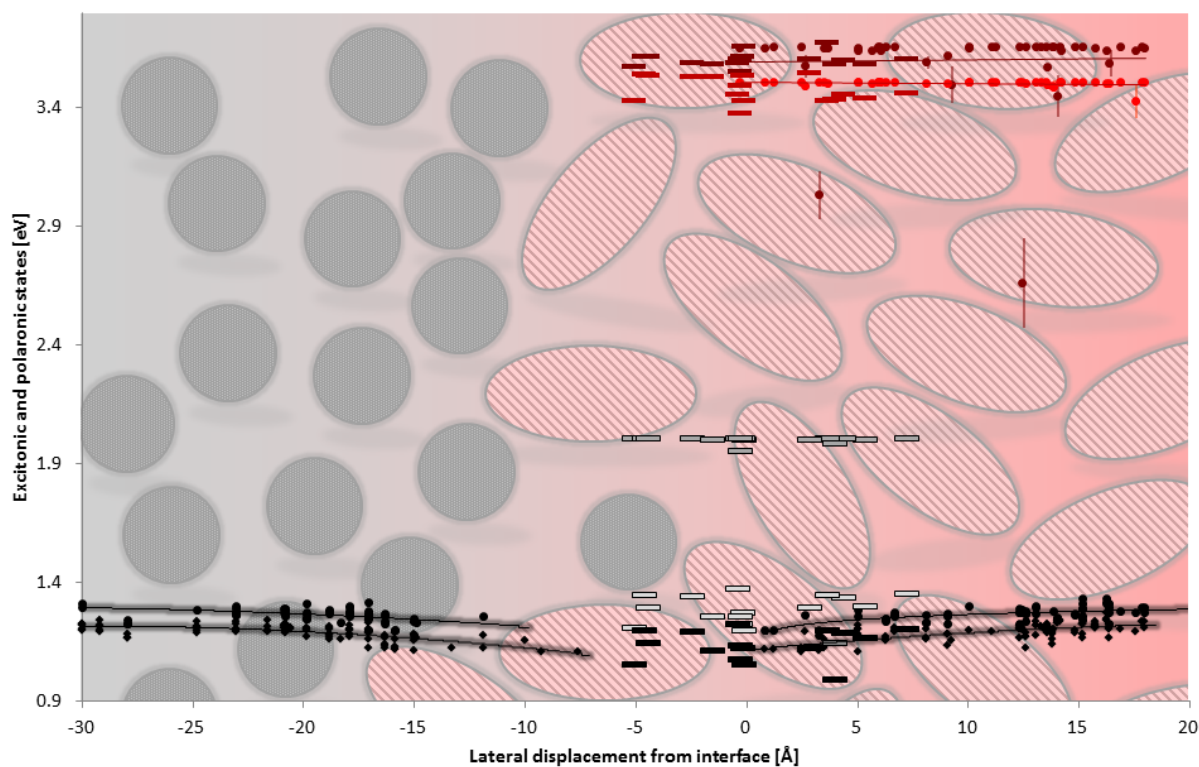


Figure S19: Energetic profile along the TBA:fullerene interface (a-b-crystallographic plane).

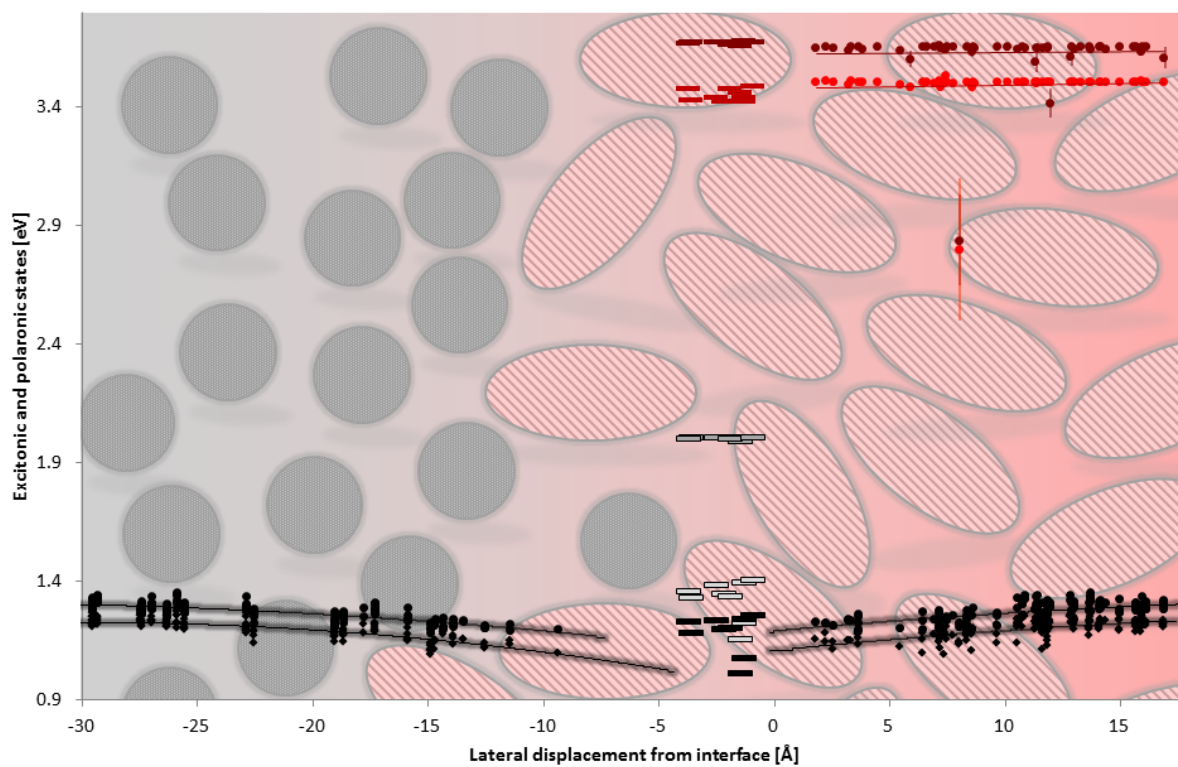


Figure S20: Energetic profile along the TBA:fullerene interface (b-c-crystallographic plane).

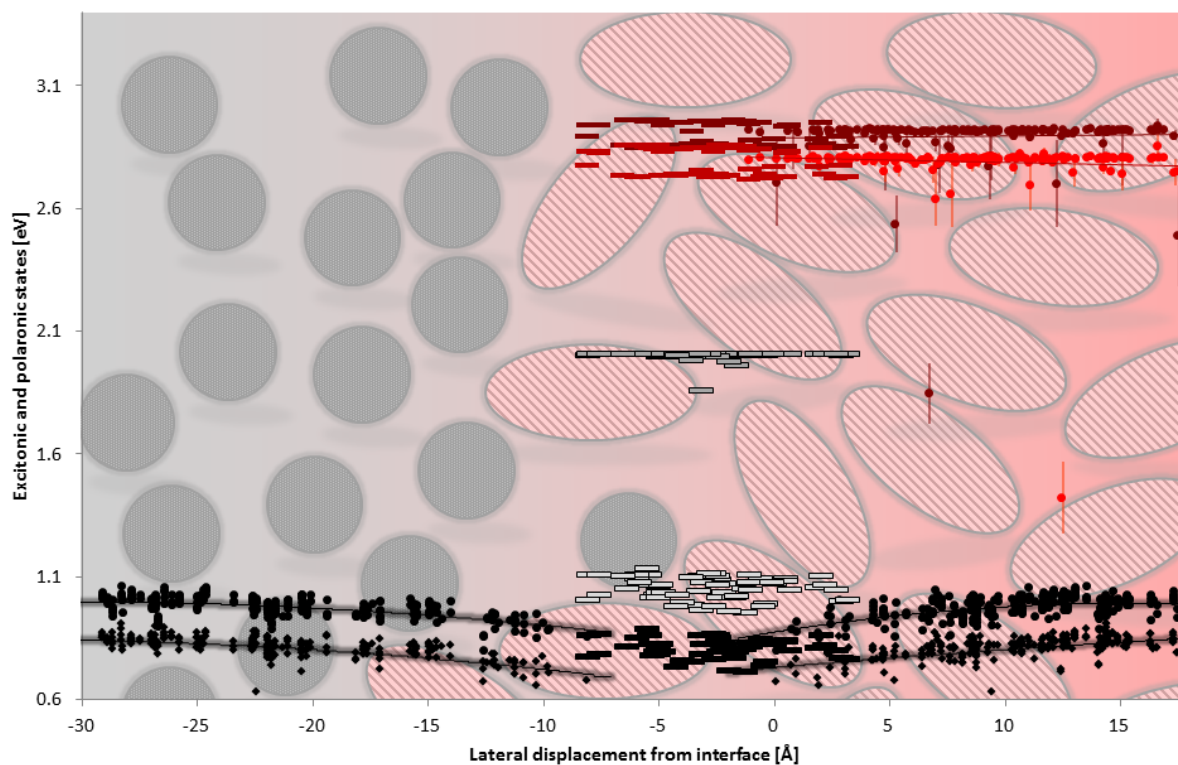


Figure S21: Energetic profile along the TAM:fullerene interface (a-c-crystallographic plane).

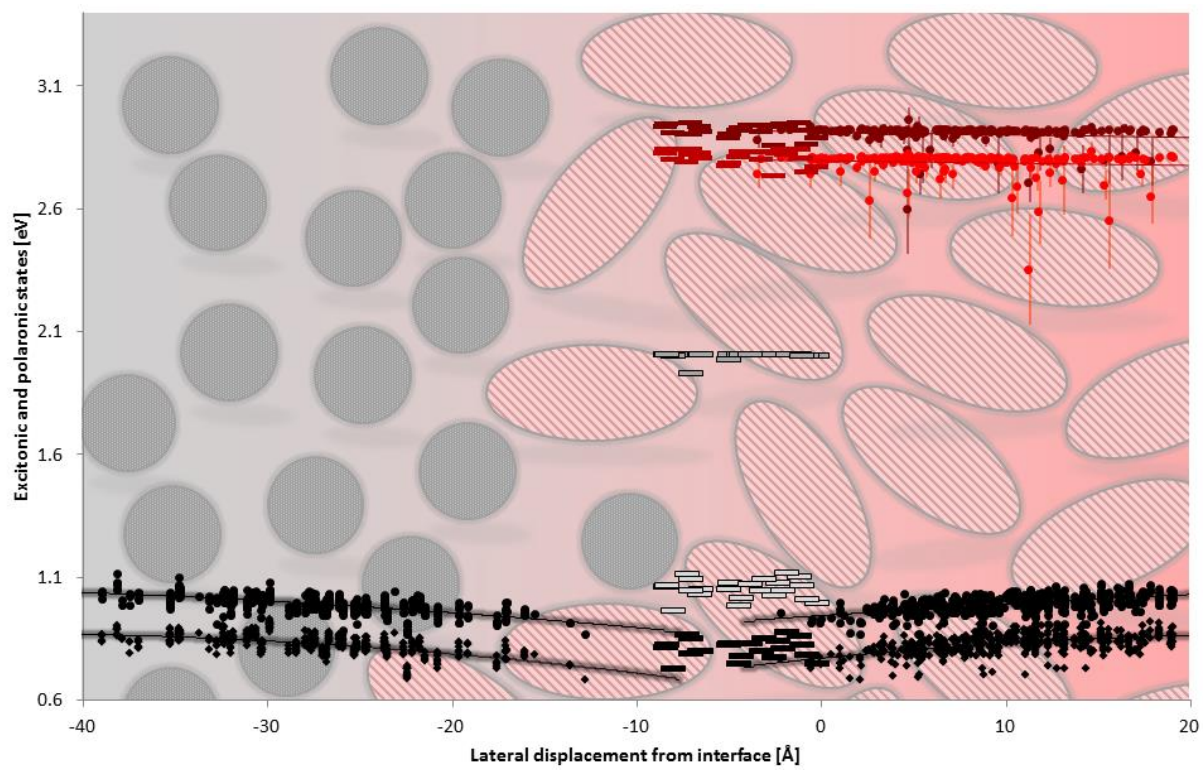


Figure S22: Energetic profile along the TAM:fullerene interface (b-c-crystallographic plane).

Influence of the interfacial electric field on the interfacial excitation energies of representative systems

To demonstrate the influence of the employed electric fields on the interfacial excitation energies, excitation energies calculated with and without the electric field are compared for four representative systems, i.e., for the interfaces composed of fullerene C₆₀ and DIP, the squaraine, the diketopyrrolopyrrole or HB194. Tables S8 through S11 display excitation energies for the four systems. Please keep in mind that interfacial excitations are neutral excitations of the donor component next to a ground-state fullerene. They are not charge-transfer excitations. The dimers are consecutively numbered with an arbitrary order.

Table S8: Interfacial excitation energies calculated with and without the electric field at the (a-c)-DIP:fullerene interface.

Dimer	interfacial exciton (vertical)		interfacial excited fullerene		interfacial exciton (relaxed)	
	with electric field [eV]	without electric field [eV]	with electric field [eV]	without electric field [eV]	with electric field [eV]	without electric field [eV]
1	2.34	2.37	1.98	2.01	1.94	1.97
2	2.35	2.37	1.98	2.01	1.96	1.97
3	2.36	2.36	1.99	2.01	1.96	1.97
4	2.36	2.36	1.98	2.01	1.96	1.96
5	2.26	2.37	1.98	2.01	1.95	1.97
6	2.34	2.37	1.98	2.01	1.95	1.97
7	2.35	2.36	1.97	2.00	1.97	1.97
8	2.34	2.36	1.97	1.99	1.95	1.97
9	2.35	2.37	1.99	2.01	1.96	1.97
10	2.34	2.36	1.98	2.01	1.95	1.97
11	2.35	2.33	1.77	1.93	1.76	1.92
12	2.33	2.37	1.99	2.01	1.94	1.97
13	2.33	2.37	1.98	2.00	1.94	1.97
14	2.33	2.37	1.98	2.01	1.94	1.97
15	2.35	2.37	1.99	2.01	1.95	1.97
16	2.34	2.37	1.98	2.00	1.95	1.97
17	2.36	2.36	1.98	2.00	1.79	1.96
18	2.35	2.37	1.98	2.00	1.95	1.97
19	2.35	2.37	1.98	2.01	1.96	1.97
20	2.35	2.37	1.99	2.01	1.96	1.97
21	2.36	2.36	1.99	2.01	1.96	1.97
22	2.36	2.37	1.99	2.01	1.92	1.97
23	2.35	2.37	1.98	2.01	1.96	1.97
24	2.35	2.37	1.98	2.01	1.96	1.97
25	2.35	2.37	1.99	2.01	1.95	1.97
26	2.36	2.37	1.99	2.01	1.96	1.97
27	2.35	2.37	1.99	2.01	1.96	1.97
28	2.36	2.36	1.98	2.01	1.96	1.97
29	2.39	2.36	1.98	2.01	1.96	1.97

30	2.39	2.33	1.94	1.99	1.72	1.94
31	2.36	2.37	1.99	2.01	1.96	1.97
32	2.36	2.36	1.98	2.01	1.96	1.97

Table S9: Interfacial excitation energies calculated with and without the electric field at the (a-c)-HB194:fullerene interface.

Dimer	interfacial exciton (vertical)		interfacial excited fullerene		interfacial exciton (relaxed)	
	with electric field [eV]	without electric field [eV]	with electric field [eV]	without electric field [eV]	with electric field [eV]	without electric field [eV]
1	2.15	2.33	1.96	1.97	2.00	2.18
2	2.16	2.34	1.98	2.00	2.01	2.18
3	2.23	2.34	1.97	1.97	2.06	2.18
4	2.23	2.34	1.99	2.01	2.06	2.18
5	2.25	2.29	1.85	1.84	2.25	2.16
6	2.25	2.34	1.99	2.01	2.09	2.18
7	2.21	2.34	1.99	2.01	2.05	2.18
8	2.21	2.34	1.99	2.01	2.05	2.18
9	2.20	2.34	1.99	2.01	2.03	2.18
10	2.16	2.34	1.99	2.01	2.01	2.18
11	2.35	2.35	1.99	2.01	2.19	2.19
12	2.49	2.34	1.99	2.01	2.33	2.18
13	2.47	2.34	1.99	2.01	2.31	2.18
14	2.25	2.05	1.70	1.72	1.73	2.17
15	2.10	2.34	1.99	2.01	1.96	2.18
16	2.08	2.34	1.99	2.01	1.94	2.18
17	2.09	2.34	1.99	2.01	1.95	2.18
18	2.14	2.34	1.99	2.01	1.98	2.18
19	2.14	2.34	1.99	2.01	1.98	2.18
20	2.30	2.31	1.95	1.96	2.16	2.15
21	2.54	2.34	1.99	2.01	2.38	2.18
22	2.46	2.34	1.99	2.01	2.30	2.18
23	2.44	2.34	1.99	2.01	2.28	2.18
24	2.38	2.34	1.99	2.01	2.22	2.18
25	2.52	2.34	1.99	2.01	2.36	2.18

Table S10: Interfacial excitation energies calculated with and without the electric field at the (a-c)-Diketopyrrolopyrrole:fullerene interface.

Dimer	interfacial exciton (vertical)		interfacial exciton (relaxed)	
	with electric field [eV]	without electric field [eV]	with electric field [eV]	without electric field [eV]
1	1.80	1.81	1.41	1.42

2	1.80	1.81	1.41	1.42
3	1.80	1.81	1.41	1.42
4	1.80	1.81	1.41	1.42
5	1.80	1.81	1.41	1.42
6	1.80	1.81	1.41	1.42
7	1.79	1.81	1.40	1.42
8	1.79	1.81	1.40	1.42
9	1.79	1.81	1.40	1.42
10	1.81	1.81	1.42	1.42
11	1.81	1.81	1.42	1.42
12	1.81	1.81	1.42	1.42
13	1.79	1.81	1.36	1.40
14	1.76	1.81	1.38	1.42
15	1.81	1.81	1.42	1.42
16	1.79	1.81	1.40	1.42
17	1.79	1.81	1.40	1.42
18	1.79	1.81	1.40	1.42
19	1.81	1.81	1.43	1.42
20	1.81	1.81	1.43	1.42
21	1.81	1.81	1.43	1.42
22	1.81	1.81	1.43	1.42
23	1.81	1.81	1.42	1.42
24	1.81	1.81	1.42	1.42
25	1.78	1.81	1.39	1.42
26	1.78	1.81	1.39	1.42
27	1.78	1.81	1.39	1.42
28	1.78	1.81	1.38	1.42

Table S11: Interfacial excitation energies calculated with and without the electric field at the (a-c)-Squaraine:fullerene interface.

Dimer	interfacial exciton (vertical)		interfacial exciton (relaxed)	
	with electric field [eV]	without electric field [eV]	with electric field [eV]	without electric field [eV]
1	1.77	1.78	1.74	1.74
2	1.78	1.78	1.75	1.75
3	1.77	1.77	1.74	1.74
4	1.77	1.77	1.74	1.74
5	1.77	1.77	1.74	1.74
6	1.77	1.77	1.74	1.74
7	1.78	1.78	1.75	1.74
8	1.77	1.77	1.74	1.74
9	1.77	1.77	1.74	1.74
10	1.77	1.77	1.74	1.74

11	1.77	1.77	1.74	1.74
12	1.77	1.77	1.74	1.74
13	1.78	1.77	1.75	1.74
14	1.77	1.77	1.74	1.74

The values in Tables S8-S11 clearly demonstrate that the influence of the electric field on the interfacial excitation energies is rather limited for all molecules except for the merocyanine HB194. Depending on the orientation of the electric field with respect to the molecular axis of HB194, excitation energies change up to 0.20-0.30 eV. However, this pronounced dependency of valence excitations on the dielectric environment is a particularity of merocyanine dyes, which possess dipolar excited states and are commonly subject to solvatochromism.^{7,27}

7. Evaluation of the calculated interfacial charge-transfer energies

Constrained density functional theory (c-DFT)²⁸ was shown to provide very accurate charge-transfer energies of organic donor-acceptor pairs.²⁹ However, calculating all interfacial charge-transfer energies with c-DFT would be computationally too demanding, the more so as donors with more than 100 atoms are involved. We therefore employed the approximate scheme defined in Eq. 5 based on the electron affinity, the ionization potential, and the Coulomb attraction.

$$E_{charge\ transfer} = IP^{p-type}(heterodimer) - EA^{n-type}(heterodimer) - \frac{e^2}{4\pi\epsilon_0\epsilon|\vec{r}|} \quad (\text{Eq. 5})$$

The ionization potential and the electron affinity are calculated as energy differences between differently charged states of the underlying heterodimer.

$$IP^{p-type}(heterodimer) = energy(heterodimer) - energy(cationic\ heterodimer) \quad (\text{Eq. 6})$$

$$EA^{n-type}(heterodimer) = energy(anionic\ heterodimer) - energy(heterodimer) \quad (\text{Eq. 7})$$

To evaluate this approximate scheme, we performed c-DFT calculations on the charge-transfer energies of a large number of heterodimers situated along the (a-b)-, (a-c)-, and (b-c)-interface of the anthracene:fullerene system. The B3LYP-D3^{10,24,30,12,11,13} functional and the cc-pVDZ¹⁴ basis sets were employed. To guarantee convergence, the computations were conducted in the gas phase. The NWChem program³¹ package was employed.

Resulting c-DFT gas-phase charge-transfer energies cannot be numerically compared to the charge-transfer energies obtained from Eq. 5 because the latter are obtained in a polarizable continuum environment. However, as already mentioned, this investigation focusses rather on correct trends than on correct numerical values. Hence it is most significant that the trends of the charge-transfer energies predicted by c-DFT and by Eq. 5 are similar. Figures S23-S28 show the correlations of charge-transfer energies of anthracene-fullerene dimers obtained with c-DFT (“CT energy (c-DFT(B3LYP))”) and with Eq. 5 (“CT energy (RI-BLYP)”).

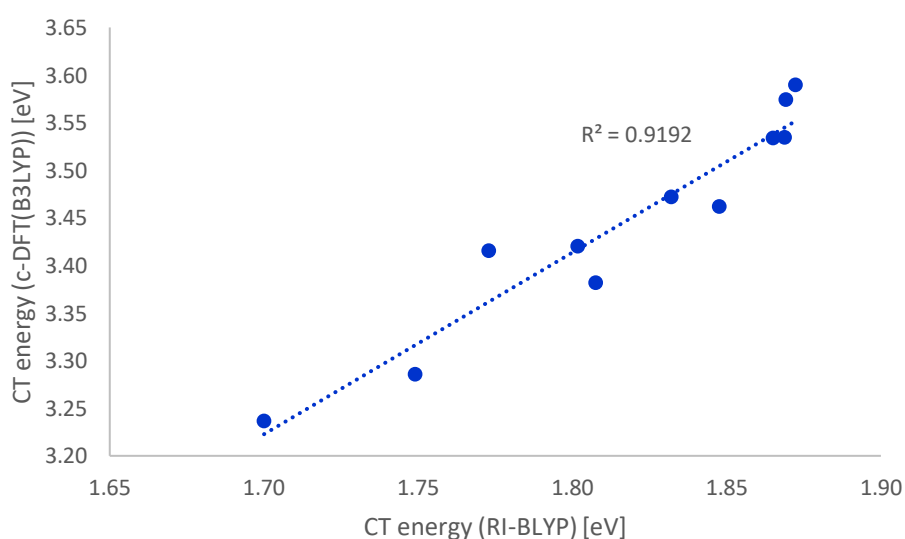


Figure S23: Comparison of vertical interfacial charge-transfer states at the (a-b)-anthracene:fullerene interface obtained with c-DFT and with Eq. 5.

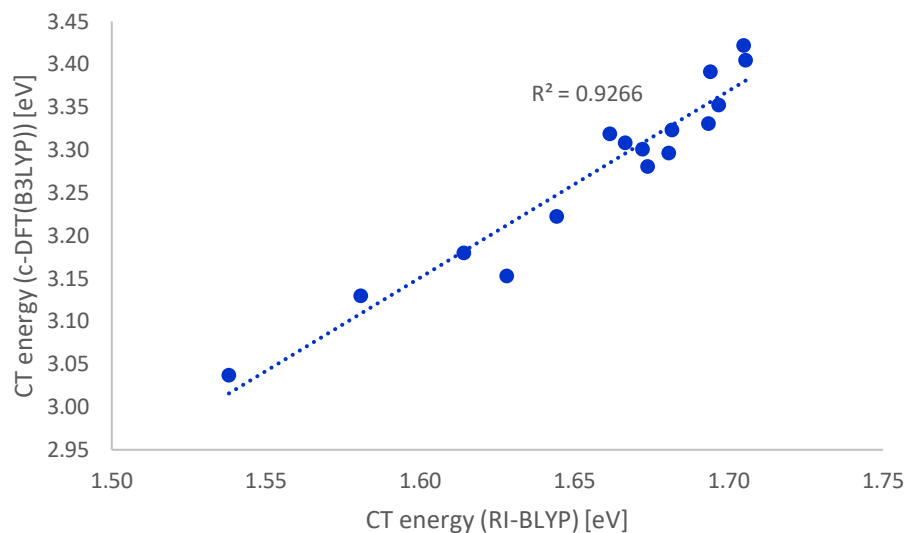


Figure S24: Comparison of relaxed interfacial charge-transfer states at the (a-b)-anthracene:fullerene interface obtained with c-DFT and with Eq. 5.

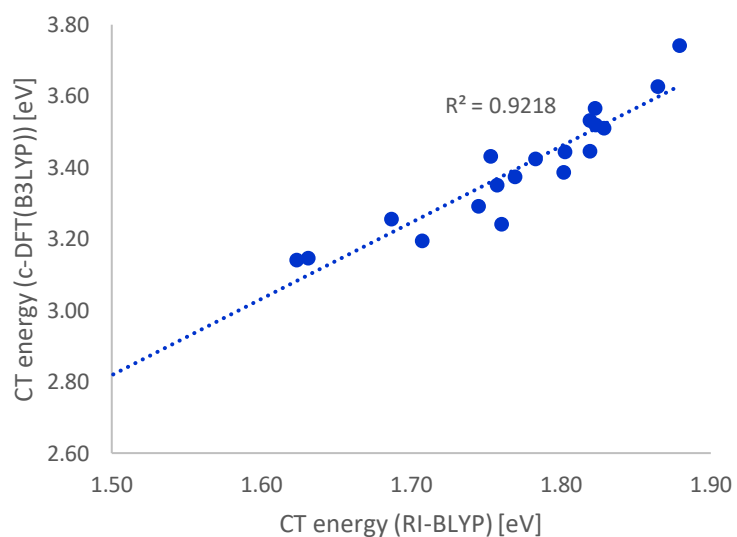


Figure S25: Comparison of vertical interfacial charge-transfer states at the (a-c)-anthracene:fullerene interface obtained with c-DFT and with Eq. 5.

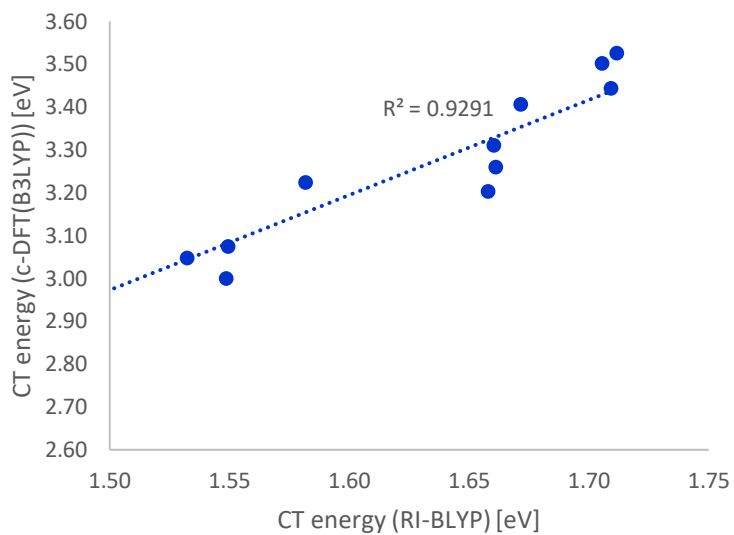


Figure S26: Comparison of relaxed interfacial charge-transfer states at the (a-c)-anthracene:fullerene interface obtained with c-DFT and with Eq. 5.

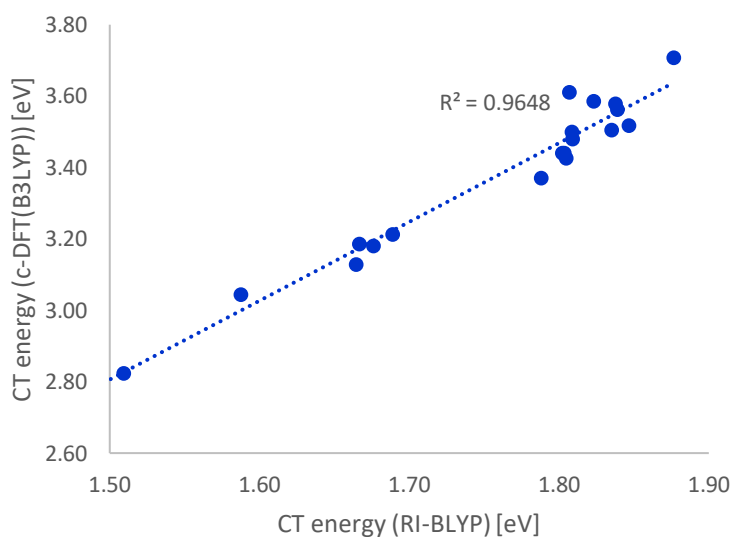


Figure S27: Comparison of vertical interfacial charge-transfer states at the (b-c)-anthracene:fullerene interface obtained with c-DFT and with Eq. 5.

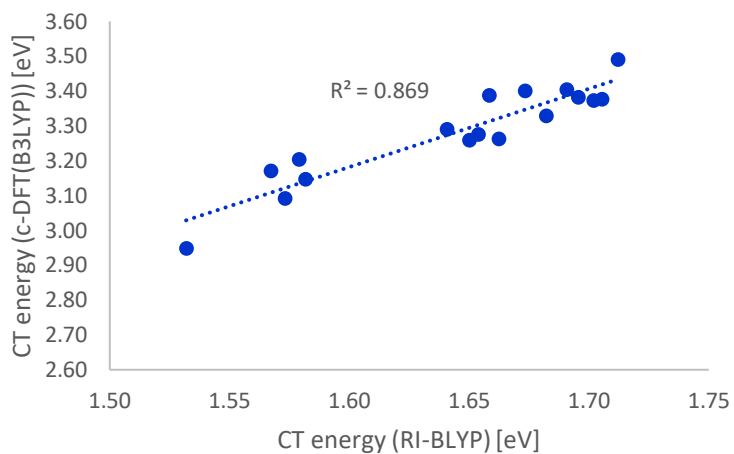


Figure S28: Comparison of relaxed interfacial charge-transfer states at the (b-c)-anthracene:fullerene interface obtained with c-DFT and with Eq. 5.

From the correlations shown in Figure S24-S28, it becomes evident that Eq. 5 and c-DFT predict similar trends for charge-transfer energies. This validates the approach.

Exemplary calculation of charge transport states at the DIP:fullerene interface

To further clarify the calculation of the charge transport states, the energy calculation of one (arbitrarily chosen) charge-transport state at the DIP:fullerene interface is described in detail in the following.

1. A dimer of DIP molecules is associated with a dimer of fullerenes. To associate them, the following conditions must be fulfilled. (1) The centers of mass of the two dimers are separated by approximately equal distances from the interfacial plane. (2) A heterodimer at the interfacial plane exists that is located approximately midway between the fullerene and the DIP dimer. It is hence assumed that a geminate pair formed on this interfacial heterodimer split up into an electron-hole pair. The electron is now situated on the fullerene dimer; the hole is located on the DIP dimer.
2. If a vertical charge-transport state is to be calculated, ground-state geometries of DIP and fullerene are used to superimpose underlying force-field geometries. If a relaxed charge-transport state is to be calculated, cationic geometries of DIP and anionic geometries of fullerene are used to superimpose underlying force-field geometries. In the model, equal geometries are always used for both monomers of any dimer, assuming that the influence of the environment on the monomer structure can be neglected. This assumption turned out to be very accurate in various previous computations about photo-induced relaxation processes.^{25,32,33}
3. Compared with the neutral ground state of the system, (1) a DIP dimer is ionized, (2) a fullerene dimer has accepted an electron, and (3) Coulomb attraction exists between the electron and the hole.
4. The ionization potential of the DIP dimer is calculated with RI-BLYP/cc-pVDZ and the MARIJ approximation as the energy difference between the cationic DIP dimer and the neutral DIP dimer both embedded in a polarizable continuum modeling the influence of the amorphous environment.
5. The electron affinity of the fullerene dimer is calculated with RI-BLYP/cc-pVDZ and the MARIJ approximation as the energy difference between the neutral fullerene dimer and the anionic fullerene dimer embedded in a polarizable continuum solvent.
6. The Coulomb attraction is calculated as the electron-hole interaction between the centers of mass of the DIP dimer and the fullerene dimer. The permittivity of the polarizable continuum solvent is taken into account.
7. Summing up the three contributions yields one charge transport state energy (=one polaronic energy). If a relaxed transport state is calculated, the ground-state reorganization is additionally added (because of the neutral ground-state reference).
8. The calculated charge-transport energy is twice incorporated into the diagrams. (1) The position of the center of mass of the DIP dimer is used to represent a transport state for a hole in the donor phase (right-hand side). (2) The position of the center of mass of the fullerene dimer is employed to display a transport state for an electron in the fullerene phase (left-hand side).

Outline of adopted methods used to calculate the states

Table S12 gives a summary of how the different states contained in the diagrams are calculated.

State	Symbol	QM	Environment
bulk excitations			
bulk exciton (vertical)		ZINDO on homodimers composed of SCS-CC2/cc-pVDZ ground-state monomer geometries	PCM
bulk exciton (relaxed)		ZINDO on homodimers composed of SCS-CC2/cc-pVDZ excited-state monomer geometries	PCM
interfacial excitations			
interfacial exciton (vertical)		ZINDO on heterodimers composed of an SCS-CC2/cc-pVDZ ground-state donor and an SCS-CC2/cc-pVDZ ground-state fullerene	PCM + electric field
interfacial exciton (=donor) (relaxed)		ZINDO on heterodimers composed of an SCS-CC2/cc-pVDZ excited-state donor and an SCS-CC2/cc-pVDZ ground-state fullerene	PCM + electric field
interfacial excited fullerene		ZINDO on heterodimers composed of an SCS-CC2/cc-pVDZ ground-state donor and an SCS-CC2/cc-pVDZ ground-state fullerene	PCM + electric field
polarons			
polaron (vertical)		RI-BLYP/cc-pVDZ (+ MARIJ) on pairs of fullerene and donor homodimers composed of monomers in their SCS-CC2/cc-pVDZ ground-state geometries <i>calculation of ionization potential and electron affinity as energy differences of</i>	PCM

		<i>differently charged states of the respective dimers</i>	
polaron (relaxed)	◆	RI-BLYP/cc-pVDZ (+ MARIJ) on pairs of fullerene and donor homodimers composed of monomers in their ω B97X-D/cc-pVDZ charged-state geometries <i>calculation of ionization potential and electron affinity as energy differences of differently charged states of the respective dimers</i>	PCM
interfacial charge transfer			
charge-transfer state (vertical)	■	RI-BLYP/cc-pVDZ (+ MARIJ) on heterodimer composed of monomers in their SCS-CC2/cc-pVDZ ground-state geometries <i>calculation of ionization potential and electron affinity as energy differences of differently charged states of the same heterodimer</i>	PCM (reduced to 50% because of next-neighbor interactions)
charge-transfer state (relaxed)	■	RI-BLYP/cc-pVDZ (+ MARIJ) on heterodimers composed of monomers in their ω B97X-D/cc-pVDZ charged-state geometries <i>calculation of ionization potential and electron affinity as energy differences of differently charged states of the same heterodimer</i>	PCM (reduced to 50% because of next-neighbor interactions)

Mass densities of generated interfacial model systems and comparison to bulk-phase densities

Table S13 displays the mass densities of the bulk crystal structures of all employed semiconducting molecules. For references see Figure 1.

Table S13: Mass densities of crystal structures.

Semiconductor	density [g/cm ³]
anthracene	1.27
rubrene	1.27
DIP	1.29
squaraine	1.12
diketopyrrolopyrrole	1.31
triphenylamine (TBA)	1.21
methoxy-sub. triphenylamine (TAM)	1.30
aldehyde-sub. triphenylamine (TAA)	1.28
MD353	1.23
HB194	1.31
fullerene	1.73

Using approximate volumes of our interfacial model systems (due to their amorphous and non-periodic nature), we calculated mass densities of our interfacial model systems (Table S14). It should be noted that the volumes employed in the density calculations are an upper bound to the real volume of the amorphous systems because we fitted rectangular boxes to the interfacial model systems. This implies that resulting densities are a lower bound.

We focused exclusively on the immediate vicinity of the interface.

Table S14: Mass densities of interfacial model systems.

System	Crystallographic orientation	density [g/cm ³]
anthracene	a-b	1.01
	a-c	0.94
	b-c	0.88
rubrene	a-b	1.14
	a-c	1.04
	b-c	1.37
DIP	a-b	1.17
	a-c	0.98
	b-c	0.80
squaraine	a-b	0.72
	a-c	1.35
	b-c	0.75
diketopyrrolopyrrole	a-b	1.18
	a-c	1.42
	b-c	1.50
triphenylamine (TBA)	a-b	0.74

	a-c	1.57
	b-c	0.74
methoxy-sub. triphenylamine (TAM)	a-b	1.16
	a-c	0.81
	b-c	0.67
aldehyde-sub. triphenylamine (TAA)	a-b	1.00
	a-c	1.18
	b-c	1.01
MD353	a-b	0.85
	a-c	1.28
	b-c	1.07
HB194	a-b	1.23
	a-c	0.75
	b-c	0.73

From the values in Table S14, it is evident that the densities in the immediate vicinity of the interfaces are reduced with respect to the crystal densities. However, this is in line with the available literature. The poor and hence less dense packing at organic:organic interfaces has for example been stressed by Van Voorhis et al.²⁹ (see also ⁸ and references therein) and by Nelson et al.³⁴ Experimental evidence was provided by Seki et al.³⁵ Our densities are also subject to considerably variations. This result similarly coincides with findings of Schröder et al.³⁶ who furthermore emphasized that only limited experimental data is available on the packing configurations at organic:organic interfaces. Heeger and coworkers experimentally found considerable mass density variations at interfaces in bulk heterojunction (BHJ) solar cells as well.³⁷ Jen et al. pointed furthermore out that the crystallization of fullerenes in BHJ cells can lead to a reduction of the interfacial density.³⁸

Moreover, it should be noted that a reduction of the density compared to the crystal phase does not only result from the nearby interface, but also from the amorphous character of the thin films. Experimental evidence for lower densities in amorphous films was provided by Lai and coworkers.³⁹ A recent computation investigation by Risko and Brédas et al.⁴⁰ furthermore demonstrated how small fullerene adducts can produce significant density variations and change the balance between inter- and intralayer polarization.

References

- (1) Klamt, A.; Jonas, V. Treatment of the Outlying Charge in Continuum Solvation Models. *J. Chem. Phys.* **1996**, *105* (22), 9972.
- (2) Klamt, A.; Schuurmann, G. COSMO: A New Approach to Dielectric Screening in Solvents with Explicit Expressions for the Screening Energy and Its Gradient. *J. Chem. Soc. Perkin Trans. 2* **1993**, No. 5, 799.
- (3) Tomasi, J.; Mennucci, B.; Cammi, R. Quantum Mechanical Continuum Solvation Models. *Chem. Rev.* **2005**, *105* (8), 2999–3093.
- (4) Bandyopadhyay, P.; Gordon, M. S.; Mennucci, B.; Tomasi, J. An Integrated Effective Fragment—polarizable Continuum Approach to Solvation: Theory and Application to Glycine. *J. Chem. Phys.* **2002**, *116* (12), 5023.
- (5) Hebard, A. F.; Haddon, R. C.; Fleming, R. M.; Kortan, A. R. Deposition and Characterization of Fullerene Films. *Appl. Phys. Lett.* **1991**, *59* (17), 2109.
- (6) Zope, R. R.; Baruah, T.; Pederson, M. R.; Dunlap, B. I. Static Dielectric Response of Icosahedral Fullerenes from C 60 to C 2160 Characterized by an All-Electron Density Functional Theory. *Phys. Rev. B* **2008**, *77* (11), 115452.
- (7) Brückner, C.; Walter, C.; Stolte, M.; Braïda, B.; Meerholz, K.; Würthner, F.; Engels, B. Structure–Property Relationships for Exciton and Charge Reorganization Energies of Dipolar Organic Semiconductors: A Combined Valence Bond Self-Consistent Field and Time-Dependent Hartree-Fock and DFT Study of Merocyanine Dyes. *J. Phys. Chem. C* **2015**, *119* (31), 17602–17611.
- (8) Yost, S. R.; Wang, L.-P.; Van Voorhis, T. Molecular Insight Into the Energy Levels at the Organic Donor/Acceptor Interface: A Quantum Mechanics/Molecular Mechanics Study. *J. Phys. Chem. C* **2011**, *115* (29), 14431–14436.
- (9) Häser, M.; Ahlrichs, R. Improvements on the Direct SCF Method. *J. Comput. Chem.* **1989**, *10* (1), 104–111.
- (10) Becke, A. D. Density-Functional Exchange-Energy Approximation with Correct Asymptotic Behavior. *Phys. Rev. A* **1988**, *38* (6), 3098–3100.
- (11) Miehlich, B.; Savin, A.; Stoll, H.; Preuss, H. Results Obtained with the Correlation Energy Density Functionals of Becke and Lee, Yang and Parr. *Chem. Phys. Lett.* **1989**, *157* (3), 200–206.
- (12) Lee, C.; Yang, W.; Parr, R. G. Development of the Colle-Salvetti Correlation-Energy Formula into a Functional of the Electron Density. *Phys. Rev. B* **1988**, *37* (2), 785–789.
- (13) Grimme, S.; Antony, J.; Ehrlich, S.; Krieg, H. A Consistent and Accurate Ab Initio Parametrization of Density Functional Dispersion Correction (DFT-D) for the 94 Elements H–Pu. *J. Chem. Phys.* **2010**, *132* (15), 154104.
- (14) Dunning, T. H. Gaussian Basis Sets for Use in Correlated Molecular Calculations. I. The Atoms Boron through Neon and Hydrogen. *J. Chem. Phys.* **1989**, *90* (2), 1007.
- (15) Sierka, M.; Hogekamp, A.; Ahlrichs, R. Fast Evaluation of the Coulomb Potential for Electron Densities Using Multipole Accelerated Resolution of Identity Approximation. *J. Chem. Phys.* **2003**, *118* (20), 9136.
- (16) Hamann, C. H.; Hamnett, A.; Vielstich, W. *Electrochemistry*, 2nd edition; WILEY-VCH Verlag GmbH: Weinheim, 2007.
- (17) David, W. I. F.; Ibberson, R. M.; Matthewman, J. C.; Prassides, K.; Dennis, T. J. S.; Hare, J. P.; Kroto, H. W.; Taylor, R.; Walton, D. R. M. Crystal Structure and Bonding of Ordered C60.

- Nature* **1991**, *353* (6340), 147–149.
- (18) Linares, M.; Beljonne, D.; Cornil, J.; Lancaster, K.; Brédas, J.-L.; Verlaak, S.; Mityashin, A.; Heremans, P.; Fuchs, A.; Lennartz, C.; et al. On the Interface Dipole at the Pentacene–Fullerene Heterojunction: A Theoretical Study. *J. Phys. Chem. C* **2010**, *114* (7), 3215–3224.
- (19) Jorgensen, W. L.; Maxwell, D. S.; Tirado-Rives, J. Development and Testing of the OPLS All-Atom Force Field on Conformational Energetics and Properties of Organic Liquids. *J. Am. Chem. Soc.* **1996**, *118* (45), 11225–11236.
- (20) Jorgensen, W. L.; Tirado-Rives, J. The OPLS [Optimized Potentials for Liquid Simulations] Potential Functions for Proteins, Energy Minimizations for Crystals of Cyclic Peptides and Crambin. *J. Am. Chem. Soc.* **1988**, *110* (6), 1657–1666.
- (21) Hirshfeld, F. L. Bonded-Atom Fragments for Describing Molecular Charge Densities. *Theor. Chim. Acta* **1977**, *44* (2), 129–138.
- (22) Marenich, A. V.; Jerome, S. V.; Cramer, C. J.; Truhlar, D. G. Charge Model 5: An Extension of Hirshfeld Population Analysis for the Accurate Description of Molecular Interactions in Gaseous and Condensed Phases. *J. Chem. Theory Comput.* **2012**, *8* (2), 527–541.
- (23) Singh, U. C.; Kollman, P. A. An Approach to Computing Electrostatic Charges for Molecules. *J. Comput. Chem.* **1984**, *5* (2), 129–145.
- (24) Becke, A. D. Density-Functional Thermochemistry. IV. A New Dynamical Correlation Functional and Implications for Exact-Exchange Mixing. *J. Chem. Phys.* **1996**, *104* (3), 1040.
- (25) Settels, V.; Schubert, A.; Tafipolski, M.; Liu, W.; Stehr, V.; Topczak, A. K.; Pflaum, J.; Deibel, C.; Fink, R. F.; Engel, V.; et al. Identification of Ultrafast Relaxation Processes As a Major Reason for Inefficient Exciton Diffusion in Perylene-Based Organic Semiconductors. *J. Am. Chem. Soc.* **2014**, *136* (26), 9327–9337.
- (26) Jensen, F. *Introduction to Computational Chemistry*, Second Edi.; John Wiley & Sons Ltd: Chichester, 2007.
- (27) Würthner, F. Dipole–Dipole Interaction Driven Self-Assembly of Merocyanine Dyes: From Dimers to Nanoscale Objects and Supramolecular Materials. *Acc. Chem. Res.* **2016**, *49* (5), 868–876.
- (28) Wu, Q.; Van Voorhis, T. Direct Optimization Method to Study Constrained Systems within Density-Functional Theory. *Phys. Rev. A* **2005**, *72* (2), 24502.
- (29) Yost, S. R.; Hontz, E.; McMahon, D. P.; Van Voorhis, T. Electronic and Optical Properties at Organic/organic Interfaces in Organic Solar Cells. *Top. Curr. Chem.* **2014**, *352*, 103–150.
- (30) Becke, A. D. Density-Functional Thermochemistry. III. The Role of Exact Exchange. *J. Chem. Phys.* **1993**, *98* (7), 5648.
- (31) Valiev, M.; Bylaska, E. J.; Govind, N.; Kowalski, K.; Straatsma, T. P.; Van Dam, H. J. J.; Wang, D.; Nieplocha, J.; Apra, E.; Windus, T. L.; et al. NWChem: A Comprehensive and Scalable Open-Source Solution for Large Scale Molecular Simulations. *Comput. Phys. Commun.* **2010**, *181* (9), 1477–1489.
- (32) Schubert, A.; Settels, V.; Liu, W.; Würthner, F.; Meier, C.; Fink, R. F.; Schindlbeck, S.; Lochbrunner, S.; Engels, B.; Engel, V. Ultrafast Exciton Self-Trapping upon Geometry Deformation in Perylene-Based Molecular Aggregates. *J. Phys. Chem. Lett.* **2013**, *4* (5), 792–796.
- (33) Zhao, H.-M.; Pfister, J.; Settels, V.; Renz, M.; Kaupp, M.; Dehm, V. C.; Würthner, F.; Fink, R. F.; Engels, B. Understanding Ground- and Excited-State Properties of Perylene Tetracarboxylic Acid Bisimide Crystals by Means of Quantum Chemical Computations. *J. Am. Chem. Soc.* **2009**,

- 131 (43), 15660–15668.
- (34) Few, S.; Frost, J. M.; Nelson, J. Models of Charge Pair Generation in Organic Solar Cells. *Phys. Chem. Chem. Phys.* **2015**, *17* (4), 2311–2325.
- (35) Akaike, K.; Kanai, K.; Uchi, Y.; Seki, K. Impact of Ground-State Charge Transfer and Polarization Energy Change on Energy Band Offsets at Donor/Acceptor Interface in Organic Photovoltaics. *Adv. Funct. Mater.* **2010**, *20* (5), 715–721.
- (36) Pfannmöller, M.; Flügge, H.; Benner, G.; Wacker, I.; Sommer, C.; Hanselmann, M.; Schmale, S.; Schmidt, H.; Hamprecht, F. A.; Rabe, T.; et al. Visualizing a Homogeneous Blend in Bulk Heterojunction Polymer Solar Cells by Analytical Electron Microscopy. *Nano Lett.* **2011**, *11* (8), 3099–3107.
- (37) Moon, J. S.; Jo, J.; Heeger, A. J. Nanomorphology of PCDTBT:PC70BM Bulk Heterojunction Solar Cells. *Adv. Energy Mater.* **2012**, *2* (3), 304–308.
- (38) Zhang, Y.; Yip, H.-L.; Acton, O.; Hau, S. K.; Huang, F.; Jen, A. K.-Y. A Simple and Effective Way of Achieving Highly Efficient and Thermally Stable Bulk-Heterojunction Polymer Solar Cells Using Amorphous Fullerene Derivatives as Electron Acceptor. *Chem. Mater.* **2009**, *21* (13), 2598–2600.
- (39) Xiang, H.-F.; Xu, Z.-X.; Roy, V. A. L.; Che, C.-M.; Lai, P. T. Method for Measurement of the Density of Thin Films of Small Organic Molecules. *Rev. Sci. Instrum.* **2007**, *78* (3), 34104.
- (40) Ryno, S. M.; Risko, C.; Brédas, J.-L. Impact of Molecular Orientation and Packing Density on Electronic Polarization in the Bulk and at Surfaces of Organic Semiconductors. *ACS Appl. Mater. Interfaces* **2016**, *8* (22), 14053–14062.